PROTON RESONANCE IN NEMATIC LIQUID CRYSTALS

By

Piyare Lal Jain

AN ABSTRACT

Submitted to the School of Graduate Studies of Michigan
State College of Agriculture and Applied Science
in partial fulfillment of the requirements
for the degree of

DOCTOR OF PHILOSOPHY

Department of Physics

1954

Approved R. D. Spence

The proton resonance line in nematic liquid crystals was detected by means of a twin-T radio frequency bridge with its conventionally associated components. The observations were made at a field of the order of 7300 gauss and at a frequency of about 31 mc.

In the normal liquid states of para-azoxyanisole and para-azoxyphenetole the line width is very narrow for both the compounds. At the transition point (135° C), between the liquid and the liquid crystal phase of para-azoxyanisole, the single line splits into three components whose peak to peak separation varies from 2.3 to 3.5 gauss throughout the entire liquid crystal range. At the second transition point (118° C) the compound passes into solid state and exhibits a wide line whose half width is of the order of 8 gauss. In para-azoxyphenetole, as in para-azoxyanisole, the single line splits into three at the transition point (166.6° C) between the liquid and the liquid crystal phase. At very low temperatures, in the liquid crystal range, five lines were observed. The peak to peak separation varies from 3 to 5.5 gauss throughout the entire liquid crystal range, and at the second transition temperature (138° C) the compound passes into the solid state and exhibits a wide line whose half width is of the order of 7 gauss.

The line structure observed in the liquid crystal range was found to be field independent and is considered to be due to the nuclear magnetic dipole interaction. The

theoretical analysis for the line shape in the liquid crystal range of these compounds has been considered with different possible orientations of the molecules under the external magnetic field. Theoretical line shape due to random orientation of the molecules with Gaussian external broadening is used to interpret the experimental line shapes. Further coincidence between experimental and theoretical values is brought through the hypothesis of partial orientation of the molecules.

PROTON RESONANCE IN NEMATIC LIQUID CRYSTALS

By

Piyare Lal Jain

A THESIS

Submitted to the School of Graduate Studies of Michigan
State College of Agriculture and Applied Science
in partial fulfillment of the requirements
for the degree of

DOCTOR OF PHILOSOPHY

Department of Physics

1954

ACKNOWLEDGEMENTS

The author wishes to express his sincere appreciation to Professor R. D. Spence for his unfailing interest and patient guidance during the course of this investigation.

VITA

Piyare Lal Jain

candidate for the degree of

Doctor of Philosophy

Final examination, May 17, 1953,

Dissertation: Proton Resonance in Nematic Liquid Crystals

Outline of Studies

Major subject: Physics
Minor subject: Mathematics

Biographical Items

Born, December 11, 1924, Punjab, India.

Undergraduate Studies, Lahore, Punjab University, 1940-44

Graduate Studies, Lahore, Punjab University, 1946-48
University of Washington, Seattle, 1949-51
Michigan State College, E. Lansing, 1951-53

Experience: Assistant, University of Washington, 1949-51
Graduate Assistant, Michigan State College, 1951-53.

Member of Sigma Pi Sigma, Society of the Sigma Xi,
The American Physical Society

TABLE OF CONTENTS

I. INTRODUCTION

A restricted group of organic substances which exhibit one or more phases intermediate to the crystalline and normal liquid phases are called liquid crystals. While they flow like ordinary liquids, they also show, in the presence of an electric or magnetic field, the anisotropy commonly associated with the crystalline state. As a result of their peculiar properties which differentiate them from liquids and solids, they have been of interest to many investigators.

If a material which exhibits a liquid crystal phase is cooled from the normal liquid phase to the liquid crystal phase, the onset of the latter phase can be easily detected by observing the change from a clear to a cloudy or milky appearance of the liquid. The study of the diffusion of polarized light through the nematic (rod like) type of liquid crystals by Par Pierre Chatelain[1] has shown that scattering is due to large particles and by comparison of the scattering in the forward and backward directions he found the dimensions of these particles to be of the order of 0.2 μ . From the X-ray study of para-azoxyanisole W. Kast[2] concludes that the groups of the molecules do not

---

1. Par Pierre Chatelain, Acta Crysta I:315 (1948)
2. W. Kast, Ann. Physik 83:418 (1927).

form straight chains but their length is undoubtedly much greater than any other dimension. Furthermore, his X-ray results agree with Stewart[3] in indicating that in the liquid crystal phase there is an aggregation of molecules much larger in size than the aggregation of molecules in the liquid phase. According to Kast[4], in the liquid crystal phase these groups of molecules or swarms, as they are called by some authors, consist of about 10^5 molecules. The molecules are rod shaped and their centers are arranged haphazardly. Monotonic liquids or those whose molecules are symmetrical in shape do not form such swarms. These swarms are considered to be equal in size but with increasing temperature they diminish in size because of the increase in thermal motion. Because of the small distance between the molecules as compared to the distance between the swarms, the interaction between the swarms is much weaker than that between the molecules in the same swarm. The direction of the swarm which is the same as the direction of the molecules in the swarm, is different from one swarm to another and will remain so unless there is some external magnetic or electric force which serves to orient them.

The swarm theory of liquid crystal phase has not been accepted by all investigators. In application the theory meets certain difficulties. It has not yet been shown

---

3. G. W. Stewart, Phy. Rev. 38:931 (1931).
4. Kast, op. cit., p. 418.

theoretically that the intermolecular forces in these substances are such as to bring about a swarm formation.

It has previously been indicated that electric or magnetic fields can cause liquid crystals to exhibit a considerable anisotropy in their physical properties. We shall now consider certain experiments which demonstrate their anisotropy and shall try to associate this anisotropy with the structure of the molecule.

Zażewski[5] has shown that dielectric constants parallel and perpendicular to the direction of the magnetic field are different. W. Mair[6] has explained the dielectric anisotropy by assuming that the magnetic field orients the molecules which in turn orient the electric dipole moments, since the electric dipole moments are fixed with respect to the molecular axes. Recent experiments[7] concerning the microwave dielectric constant have also shown that a magnetic field can produce an anisotropy in both real and imaginary parts of the dielectric constant. In both the static and dynamic dielectric constants, it has been found that the orienting effect of the magnetic field saturates at fields of the order of 1000 gauss. M. C. Mañgun[8] has studied the optical properties of liquid crystals and has

---

5. M. Zażewski, Z. Physik 40:153 (1927).
6. W. Mair, Z. Naturforschung 8:458 (August, 1947).
7. E. Carr and R. Spence, Bull. Am. Phys. Soc. 28(1):8 (1953).
8. M. G. Mañgun, Compt. rend. 152:1680 (1911).

found that they are spontaneously bi-refringent and uni-axial. When subjected to a strong magnetic field their molecules are oriented such that their optic axes are parallel to the lines of force.

Föex and Royer[9] have measured the magnetic susceptibility of several nematic liquid crystals and found that they are diamagnetic. Below the melting point the substance forms a crystalline powder which is almost isotropic. At the melting point there is a sudden decrease of the diamagnetic susceptibility. As the temperature is raised there is a small gradual increase of the diamagnetic susceptibility until the transition temperature between liquid and liquid crystal phase is reached. There is a very rapid rise in the susceptibility as the substance enters the liquid phase. The susceptibility in the liquid phase is slightly lower than the susceptibility in the crystalline phase. By supercooling, the curve for decreasing temperature can be extended to lower temperatures. At the moment of crystallization the susceptibility rises sharply to the value found in the solid state.

We now consider the origin of the diamagnetic anisotropy of these compounds. It has been observed[10] that crystals with layer-like lattices exhibit a marked anisotropy in the diamagnetic susceptibility, the susceptibility

---

9. Föex and Royer, Compt. rend. 180:1912 (1925).
10. K. S. Krishanan, Proc. Ind. Soc. Cong. Madras Session (1929).

being abnormally large when measured in a direction normal to the layers. It was pointed out by Raman and Krishanan[11] that the abnormal susceptibility probably arises from the Larmour procession of electrons in orbits including many nuclei. F. London[12] has given a quantum theoretical treatment of this effect for aromatic molecules while Pauling[13] has worked out a semiclassical theory of the effect using electrical circuit theory. In the case of aromatic molecules, he assumes that the outermost six electrons of the six-carbon atom of benzene (one per carbon atom) are free to move from one carbon atom to an adjacent carbon atom in the ring under the influence of the impressed field and give rise to extra magnetic fields in a direction normal to the plane of the benzene ring. On Pauling's model of magnetic susceptibility the value of the susceptibility will be much greater along an axis perpendicular to the plane of the benzene ring than along either of the two axes in the plane of the ring. Similarly, this model can be extended to other molecules having different combinations of benzene rings. For the case of the nematic type of liquid crystals there are two or more benzene rings. They give rise to a separate induced current in the presence of a magnetic field. This induced current results in producing

---

11. Krishanan, op. cit.
12. F. London, J. Phys. radium 8:397 (1937).
13. L. Pauling, J. Chem. Phys. 4:673 (1936).

induced magnetic fields perpendicular to the direction of the molecular axis. Föex[14] has shown that the least value of diamagnetic susceptibility is in the direction of the longer axis of the molecule, hence on the application of a magnetic field the molecules will tend to orient themselves with their long axes parallel to the field. Since nematic liquid crystals do not contain free radicals, they do not have permanent magnetic dipole moments and their orientation in the magnetic field is simply due to the presence of diamagnetism in these compounds.

All the above experimental results show that the molecules are oriented in a magnetic field in the liquid crystal phase along the direction of the magnetic field and this alignment decreases with increasing temperature until finally in the liquid state local thermal effects dominate those of the magnetic field.

According to Frankel[15] and Landau[16] the change in the phase from liquid crystal to liquid is associated with transition from an ordered to a disordered state, and there is no longer any preferred orientation of the molecules in the liquid phase. Kreutzer[17] is of the opinion that there are some motions of rotation and oscillation associated

---

14. Föex, J. de Phys. et le Rad. VI (X):421 (1929).
15. J. Frankel, Kinetic Theory of Liquids. Oxford University Press, London, 1946. Chpt. 2.
16. L. Landau, Physik. Zeits. Sowjetunion 11(26):545 (1937).
17. Kreutzer, Ann. Physik 33:192 (1938).

with the molecules when the compound is in the liquid crystal phase and that they change to free rotation in the liquid phase. His experimental results on specific heat of the nematic type of liquid crystal show a higher value in the liquid crystal phase than in the liquid phase. He considers this change due to the different types of motion associated with the different phases. He has also measured the value of the heat of transformation from the normal liquid phase to the liquid crystal phase in the nematic type of liquid crystals. From Alpert's[18] studies of the phase transition in solids by means of the nuclear magnetic resonance, it appears that one should be able to observe the phase transition of the nematic liquid crystal phase by means of proton magnetic resonance. This thesis reports the results of the study of the phase transitions and of the structure of the proton magnetic resonance line in nematic liquid crystals.

---

18. N. L. Alpert, Phys. Rev. 75:398 (1949).

II. THEORY

Dipole Dipole Interaction

In this section certain quantum mechanical results will be summarized which will ultimately be required for the explanation of the experimental work. These deal with the quantum mechanical description of the interaction between nuclear nagnetic dipoles and its effect on the shape of the nuclear magnetic resonance line.

The classical expression for the interaction energy between two dipoles situated at a distance r is given by,

$$E_{12}^{(1)} = \frac{\bar{\mu}_1 \cdot \bar{\mu}_2}{r_{12}^3} - 3\frac{\bar{\mu}_1 \cdot \bar{r}_{12}\ \bar{\mu}_2 \cdot \bar{r}_{12}}{r_{12}^5}, \qquad (1)$$

where $\bar{r}_{12}$ is the internuclear vector and

r_{12} is its magnitude,

μ_1 and μ_2 are the dipole moments corresponding to two nuclei under consideration.

Let $\bar{\mu} = g\beta\bar{S}$

where $\bar{S}$ = nuclear spin in units of $\hbar$,

g = nuclear g- factor,

β = nuclear magneton.

Eq. (1) can be written as

$$E_{12} = g_1 g_2 \beta^2 \left(\frac{\bar{S}_1 \cdot \bar{S}_2}{r_{12}^3} - 3 \frac{(\bar{S}_1 \cdot \bar{r}_{12})(\bar{S}_2 \cdot \bar{r}_{12})}{r_{12}^5} \right) . \quad (2)$$

The quantum mechanical expression for the interaction energy of two dipoles of two identical nuclei is given by the Hamiltonian

$$\mathcal{H}^{(1)} = g^2 \beta^2 \left(\frac{\bar{S}_1 \cdot \bar{S}_2}{r_{12}^3} - 3 \frac{(\bar{S}_1 \cdot \bar{r}_{12})(\bar{S}_2 \cdot \bar{r}_{12})}{r_{12}^5} \right) , \quad (3)$$

where $\bar{S}_1$ and $\bar{S}_2$ are the two nuclear spin operators.

The total interaction energy of two dipoles in the presence of an external field H_0 is given by the Hamiltonian

$$\mathcal{H} = \mathcal{H}^{(0)} + \mathcal{H}^{(1)} , \quad (4)$$

where $$\mathcal{H}^{(0)} = - g \beta H_0 \sum_{j=1}^{2} S_{zj} . \quad (5)$$

The symbol S_{zj} denotes the z-matrix component of the spin angular momentum of the nucleus of atom j, measured in multiplets of the quantum units $\hbar$.

Eq. (5) represents the Zeeman energy of the nuclear dipoles in the external field H_0, which is taken in $\bar{Z}$-direction.

Eq. (3) can be re-written as[19]

$$\mathcal{H}^{(1)} = A_{12} (\bar{S}_1 \cdot \bar{S}_2 - 3 S_{z1} S_{z2}) , \quad (6)$$

---

19. Van Vleck, Phys. Rev. 74:1168 (1948).

where $$A_{12} = \frac{1}{2}\frac{g^2\beta^2}{r_{12}^3}\left(3\cos^2\theta_{12} - 1\right).$$

θ_{12} is the angle between the external field $\overline{H_o}$ and $\overline{r}_{12}$, the vector connecting nuclei 1 and 2. For a rigid lattice the matix elements of $\mathcal{H}^{(1)}$ are computed using spin eigen functions only and treating A_{12} as constants. $\mathcal{H}^{(1)}_{(o)}$ may be treated as perturbing the Zeeman levels of $\mathcal{H}^{(1)}$, and the solution of this perturbation problem will yield the detailed structure of the absorption line. Since in our problem we shall be particularly interested in the effect of the interaction of two dipoles on their Zeeman levels, we shall write down a brief outline for computing the energy level diagram for such a case.

With the usual notation (+) and (-) represent the normalized spin eigen functions of z-component of the total spin S. For the system of a pair of nuclei the four combinations of orthonormal wave functions are

$$\begin{aligned} &(+\ +)\ , \\ &\tfrac{1}{\sqrt{2}}\left[(+-) + (-+)\right], \\ &(-\ -)\ , \\ &\tfrac{1}{\sqrt{2}}\left[(+-) - (-+)\right]. \end{aligned} \qquad (7)$$

The first three wave functions represent triplet states while the last one represents the singlet state corresponding to parallel and antiparallel spins respectively. Since

the selection rules for magnetic dipole transitions are $\Delta s = 0$ and $\Delta m = \pm 1$, the transition from the triplet to the singlet state is forbidden.

The matrix element of the Hamiltonian $\mathcal{H}^{(1)}$ are given by

$$\begin{aligned} \mathcal{H}_{11} &= -\frac{\mu^2}{r^3}(3\cos^2\theta - 1), \\ \mathcal{H}_{22} &= 2\frac{\mu^2}{r^3}(3\cos^2\theta - 1), \\ \mathcal{H}_{33} &= -\frac{\mu^2}{r^3}(3\cos^2\theta - 1), \\ \mathcal{H}_{44} &= 0, \end{aligned} \tag{8}$$

where $2\mu = g\beta$.

These are the eigen values corresponding to eigen functions described in Eq. (7). The perturbed as well as unperturbed energy levels are shown in Figure 1. Resonance absorption for the perturbed system occurs when the following conditions are satisfied.

$$m = +1 \longrightarrow m = 0$$

$$h\nu = 2\mu H_0 + 3\frac{\mu^2}{r^3}(3\cos^2\theta - 1), \tag{9}$$

$$m = 0 \longrightarrow m = -1$$

$$h\nu = 2\mu H_0 - 3\frac{\mu^2}{r^3}(3\cos^2\theta - 1). \tag{10}$$

Putting $h\nu = 2\mu H^x$ in Eqs. (9) and (10) where H^x is the resonance value for the external field, then one gets

$$H_0 = H^x \pm \frac{3}{2}\frac{\mu}{r^3}(3\cos^2\theta - 1). \tag{11}$$

This equation locates a pair of fine structure lines for each existing direction θ in the sample such that separation between these two lines is given by $\Delta H = 3\mu/r^3 (3\cos^2\theta - 1)$.

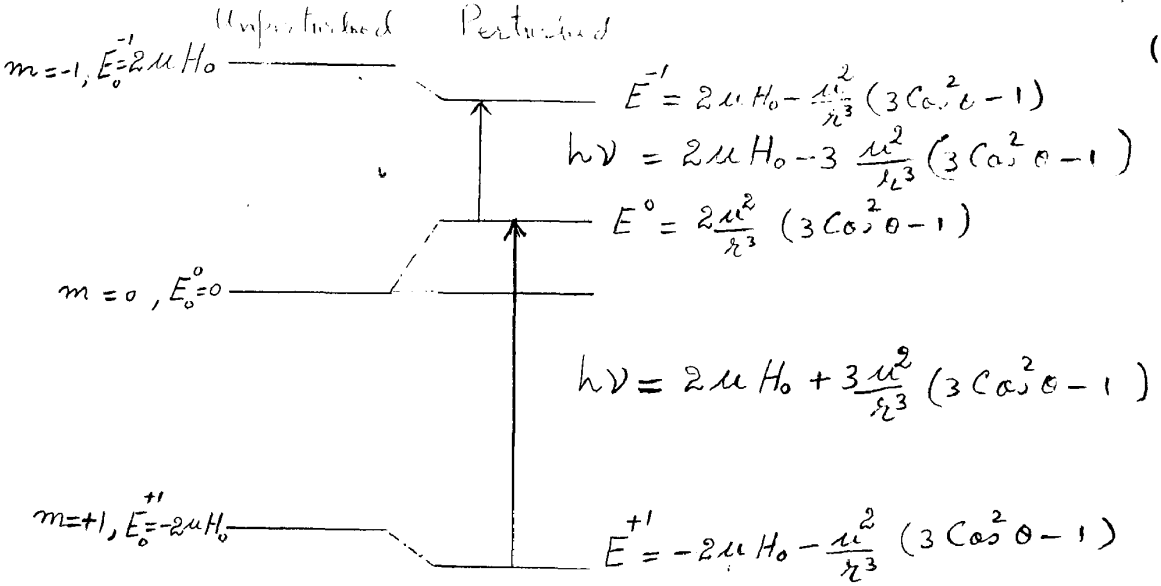

(11a)

Figure 1. Energy level diagram showing the effect of the dipole dipole interaction on the ordinary Zeeman levels E_o^m of two proton system.

Effect of Rotation on Dipolar Splitting

If the nuclei which are at resonance rotate in the crystal lattice, then energy consists of the kinetic energy of rotation together with the potential energy due to its position and spin in the lattice and the Zeeman energy of their nuclear magnetic moment,

$$\mathcal{H} = \sum_j \mathcal{H}_j = \sum_j (T_j + V_j) , \qquad (12)$$

where T_j and V_j are the kinetic and potential energy of the jth particle.

Eigen function Ψ of Eq. (12) is given by the product of spin and orbital eigen functions, that is,

$$\Psi = \prod \Psi_j ,$$

where $\Psi_j = \chi_j(s)\, u_j(\theta_j, \phi_j)$,

spin (s) and orbital (θ_j, ϕ_j) co-ordinates are independent. Total energy is given by

$$E = \int \bar{\Psi} H \Psi \, d\tau_s \, d\tau_{\theta\phi} ,$$

$$E = \sum_j \int \bar{u}_j T_j u_j \, d\tau_s + \sum_j \int \bar{u}_j \left(\int \bar{\chi}_j V_j \chi \, d\tau_{s_j} \right) u_j \, d\tau_{\theta_j \phi_j} ,$$

$$= \sum_j \langle T_j \rangle_{q.m} + \sum_j \int \bar{u}_j (v_j)\, u_j \, d\tau_{\theta,\phi} , \qquad (13)$$

where $\langle v_j \rangle_{q.m} = \int \bar{\chi}_j V_j \chi_j \, d\tau_{s_j}$.

If we suppose that quantum mechanical average $\langle v_j \rangle$ can be replaced by the classical average then

$$E \simeq \sum_j \langle T_j \rangle_{q.m} + \sum_j \langle v_j \rangle_{Class} \qquad (13a)$$

Now we consider two interacting nuclei moving about an axis perpendicular to the line joining them, as shown in Figure 2.

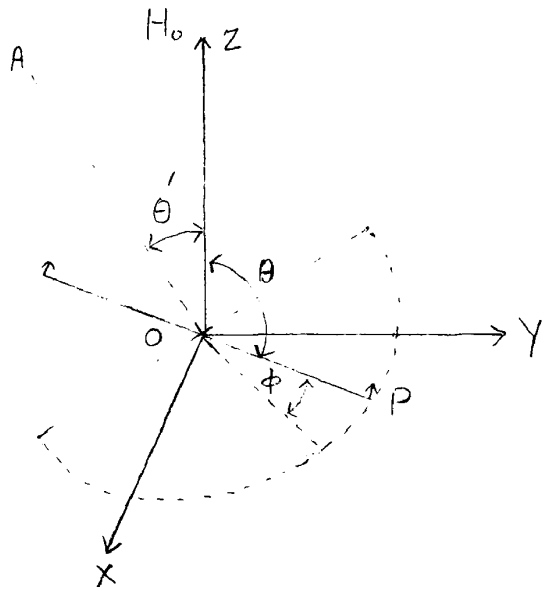

Figure 2. Model for a nuclear pair in motion about an axis perpendicular to the internuclear axis.

By the method of transformation of coordinates

$$\cos\theta = \cos\phi \sin\theta' \tag{14}$$

so that $3\cos^2\theta - 1 = 3\cos^2\phi \sin^2\theta - 1$

where ϕ is the azimuthal or rotational angle of the internuclear vector $\overline{OP}$ about the rotation axis OA which makes an angle θ' with the external field. For classical rotation where $\phi = \omega t$ the average value of $\cos^2\phi$ over the rotation is 1/2 so that

$$\begin{aligned} \langle 3\cos^2\theta - 1 \rangle_{rot} &= \langle 3\cos^2\phi \sin^2\theta' - 1 \rangle_{rot} \\ &= 3/2 \sin^2\theta' - 1 \\ &= 1/2 \left(1 - 3\cos^2\theta'\right) \end{aligned} \tag{15}$$

Eq. (11) shows that the absorption line at fixed frequency composed of two components at magnetic fields given by

$$H_o = \frac{h\nu}{g\beta} \pm 3/2 \frac{\mu}{r^3} (3\cos^2\theta - 1) . \tag{16}$$

Under the effect of rotation the two components will have values

$$H_o = \frac{h\nu}{g\beta} \pm \frac{3}{4} \frac{\mu}{r^3} (3\cos^2\theta - 1) , \tag{17}$$

and the doublet separation is half as great as for the stationary pair. In the case of a powder sample, the random orientation of microcrystals provides all values of either θ or θ' for all states of motion. Pake[20] has shown that for the case of a powder sample the doublet separation is $3\mu/r^3$ while on increasing the temperature, rotation of the molecules takes into play and thereby separation becomes half as wide as for the stationary pair, that is $3/2\,\mu/r^3$.

Calculation of the Mean Square Absorption Frequency.

The definition of mean square of ν^2 is given by

$$\langle \nu^2 \rangle = \frac{\int \nu^2 P(\nu)\, d\nu}{\int P(\nu)\, d\nu} = \frac{\Sigma_i \nu_i^2 P_i}{\Sigma_i P_i} \tag{18}$$

where $P(\nu)$ is the probability density.

---

20. G. E. Pake, J. Chem. Phys. 16:327 (1948).

In Eq. (4) $\mathcal{H}$ represents Hamiltonian matrix for the system of nuclear dipoles and S spin quantum number. If $(S_x)_{nn'}$ be the matrix element of $S_x = \sum_j S_{xj}$ which connects the states n and n', the corresponding frequency is

$$\nu_{nn'} = \frac{(\mathcal{H}_n - \mathcal{H}_{n'})}{h} \tag{19}$$

If $|(S_x)_{nn'}|^2$ is the transition probability density between the states n and n', then according to Eq. (18) the mean square absorption frequency is given by

$$\langle \nu^2 \rangle_{av} = \frac{\sum_n \sum_{n'} \nu_{nn'}^2 |(S_x)_{nn'}|^2}{\sum_n \sum_{n'} |(S_x)_{nn'}|^2} . \tag{20}$$

Both the numerator and the denominator of Eq.(20) can be expressed as diagonal sums .

Van Vleck[21] has shown that

$$\sum_n \sum_{n'} |(S_x)_{nn'}|^2 = Tr\,(S_x)^2_{nn} ,$$

$$\sum_n \sum_{n'} \nu_{nn'}^2 |(S_x)_{nn'}|^2 = -Tr\,[\mathcal{H}(S_x - S_x)\mathcal{H}]^2 ,$$

so that

$$\langle \nu^2 \rangle_{av} = -\frac{Tr\,[\mathcal{H}(S_x - S_x)\mathcal{H}]^2}{h^2\, Tr\,(S_x)^2} . \tag{21}$$

---

21. Van Vleck, op. cit., p. 1168.

He makes use of the well known theorem of the transformation theory that the trace is independent of the representation. Writing Eq. (4) in the form

$$\mathcal{H} = H_0 g \beta \sum_j S_{zj} + \sum_{k>j} A_{jk} \bar{S}_j \cdot \bar{S}_k + \sum_{k>j} B_{jk} S_{zj} S_{zk}, \qquad (22)$$

where

$$A_{jk} = \frac{g^2\beta^2}{r^3_{jk}} \left(3/2 \cos^2 \theta_{jk} - 1/2 \right) ,$$

$$B_{jk} = -\frac{3 g^2 \beta^2}{r^3_{jk}} \left(3/2 \cos^2 \theta_{jk} - 1/2 \right) .$$

The common commutation and trace relations are

$$\begin{aligned} &S_{xj} S_{yk} - S_{yk} S_{xj} = i \delta_{jk} S_{zj} , \\ &Tr\, S_z^2 = 1/3\, S(S+1)(2S+1)^N , \qquad (23) \\ &Tr\, S_{zj} = 0 , \end{aligned}$$

where S is the nuclear spin quantum number of an individual atom.

Also $Tr\, S_{xj} S_{xk} = Tr\, S_{xj} = Tr\, S_{xk} = 0 \quad (j \neq k)$, etc.

Proceeding in this fashion one finds that

$$Tr\, (S_x)^2 = \frac{1}{3} N S(S+1)(2S+1)^N ,$$

$$\mathcal{H} S_x - S_x \mathcal{H} = H g \beta i \sum_j S_{yj} + i \sum_{k>j} B_{jk} (S_{yj} S_{zk} + S_{yk} S_{zj}) ,$$

$$-\frac{Tr[\,)(S_x-S_x)(\,]^2}{(2S+1)^N} = \frac{1}{3}N\gamma^2\beta^2 HS(S+1) + \frac{2}{9}S^2(S+1)^2 \sum_{k\neq j} B_{jk}^2$$

where

$$\sum_{k>j}\sum_{k>j} B_{jk}^2 = \frac{N}{2}\sum_{k\neq j} B_{jk}^2 .$$

$\therefore$ Eq. (21) yields

$$\langle \nu^2 \rangle_{av} = -\frac{Tr[\,)(S_x-S_x)(\,]^2}{h^2\, Tr\,(S_x)^2} \qquad (24)$$

$$= -\frac{\gamma^2\beta^2H^2}{h^2} + \frac{2}{3N}\frac{S(S+1)}{h^2}\sum_{k>j} B_{jk}^2 .$$

The second moment of the absorption line is defined as the average value of $(\nu-\nu_0)^2$ over the symmetrical line shape, that is

$$\langle(\nu-\nu_0)^2\rangle_{av} = \langle(\Delta\nu)^2\rangle_{av} = \langle\nu^2\rangle_{av} - \nu_0^2 \qquad (25)$$

where $\nu_0 = H\gamma\beta/h$

$$\therefore \langle(\Delta\nu)^2\rangle_{av} = \langle\nu^2\rangle_{av} - \frac{\gamma^2\beta^2H^2}{h^2} = \frac{2}{3}\frac{S(S+1)}{N\,h^2}\sum_{k>j} B_{jk}^2,$$

$$= \frac{3}{2}\gamma^4\beta^4\frac{S(S+1)}{h^2}\sum_{k>j}\left\langle\frac{(3\cos^2\theta-1)^2}{r_{jk}^6}\right\rangle_{av} \qquad (26)$$

where N is the number of the nuclei at resonance which are present in the elementary dipole interaction cell.

The root second mean (ΔH_2) is related to $\langle(\Delta\nu^2)\rangle_{av}$ by the relation

$$\Delta H_2 = \frac{h}{g\beta}\langle(\Delta\nu^2)\rangle_{av}^{1/2} \quad . \tag{27}$$

So the value of the second moment for a particular orientation of the dipole with respect to H_0 is given by

$$\Delta H_2^2 = 3/2\ \frac{S(S+1)}{N}\ g^2\beta^2 \sum_{k\neq j} \left\langle \frac{3\cos^2\theta_{jk} - 1}{r_{jk}^6} \right\rangle_{av}^2 . \tag{28}$$

In the case of crystalline powder, the constituent microcrystals are presumed to be randomly distributed among all directions in space, so averaging over

$$\langle(3\cos^2\theta_{jk} - 1)^2\rangle_{av} = \frac{\int_0^{\pi}(3\cos^2\theta_{jk} - 1)^2 \sin\theta\, d\theta}{\int_0^{\pi}\sin\theta\, d\theta} = 4/5 . \tag{29}$$

One obtains for the case of powder sample the relation

$$\Delta H_2^2 = 6/5\ \frac{S(S+1)}{N}\ g^2\beta^2 \sum_{k\neq j} \frac{1}{r_{jk}^6} . \tag{30}$$

Effect of Rotation on the Second Moment

In Eq. (28) the pointed brackets denotes the average value of the orbital factor over the rotation.

We consider the classical rotation involving the azimuthal angle ϕ as shown in Figure 3.

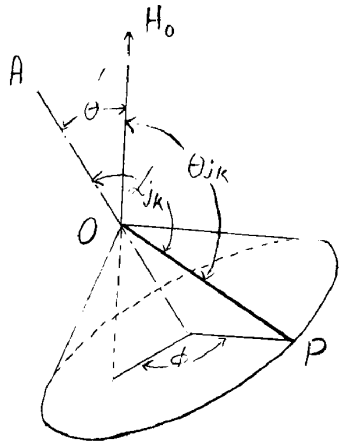

Here $\overline{OP}$ is the internuclear vector.

Figure 3. Model for a nuclear pair in motion about any axis.

For this case the addition theorem for spherical harmonies is given by

$$\langle P_\ell(\cos\theta_{jk})\rangle_\phi = P_\ell(\cos\theta')\,P_\ell(\cos\alpha_{jk}),$$

For $\ell = 2$

$$P_2(\cos\theta) = \tfrac{1}{2}(3\cos^2\theta - 1), \tag{31}$$

$$\therefore \langle(3\cos^2\theta_{jk}-1)\rangle_\phi = \tfrac{1}{2}(3\cos^2\theta'-1)(3\cos^2\alpha_{jk}-1),$$

and the second moment for a system rotating about an axis making an angle θ' with $\bar{H}_0$ is given by,

$$\Delta H_2^2 = \tfrac{1}{4}(3\cos^2\theta'-1)\left[3/2\,\frac{S(S+1)}{N}\,g^2\beta^2\sum_{j\neq k}\frac{(3\cos^2\alpha_{jk}-1)}{r_{jk}^6}\right]. \tag{32}$$

For the case of a crystal powder, the second moment is given by[22]

$$(\Delta H_2^2)_{Powder} = \frac{1}{4}\left[\frac{6}{5}\frac{S(S+1)}{N} g^2\beta^2 \sum_{j,k} \frac{(3\cos^2\alpha_{jk}-1)^2}{R_{jk}^6}\right]. \quad (33)$$

For a special case where $\alpha_{jk} = \pi/2$, that is, if the rotational axis is perpendicular to the internuclear vector then the second moment for a powder, in which such rotation occurs, is one-fourth as great as if the lattice were rigid. In general there is no simple relation between the half width of a line and the root mean square width. However, if one assumes the relation the line shape is Guassian one finds

$$\Delta H_2 = .43\,\delta H, \quad (34)$$

where ΔH_2 = root mean second moment

δH = half line width of an absorption curve.

---

22. Gutowsky and Pake, J. Chem. Phys. 18:162 (1950).

III. THE EXPERIMENTAL METHOD

The general experimental arrangement is shown in the block diagram, Figure 4. A General Radio 620-A Wave meter served as a signal generator in all the experiments. A frequency range from 300 Kc to 300 Mc was available, and the frequency could be determined accurately within one kilocycle. Most of the experimental work was done at a frequency in the neighborhood of 31 Mc. At this frequency the magnetic field strength for proton resonance was about 7300 gauss.

The output of the signal generator was fed into the twin-T bridge. An r.f. coil which contained the sample formed part of the tuned circuit of the bridge and was placed between the poles of a large electromagnet. At resonance the signal from the unbalanced bridge was amplified by either one broad band pre-amplifier or two of these amplifiers in series. After pre-amplification, the signal was detected by a Hallicrafter SX-62 receiver whose power supply was regulated electronically.

An alternating field modulated the static magnetic field, H_o. The modulating magnetic field was provided by a thirty or sixty cycle alternating voltage applied to two Helmoholtz coils mounted one on each pole piece. With the

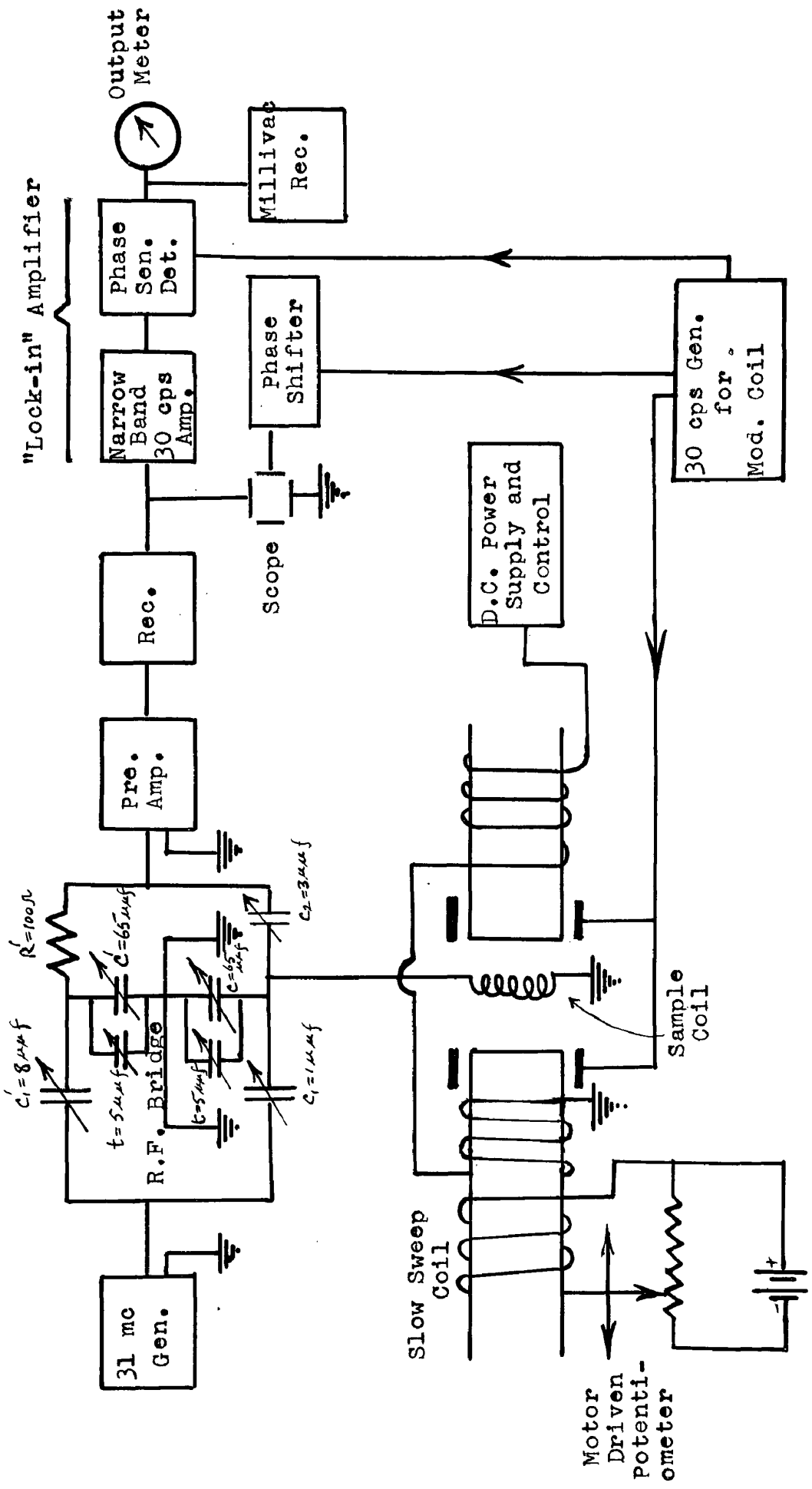

Figure 4. Block diagram

static field, H_o, near resonance, the modulating field caused H_o to pass through the resonance value either 60 or 120 times per second. Application of the resonance signal from the receiver to the vertical plates of an oscilloscope and syncronization of the sweep with the modulating voltage permitted the resonance line to be displayed on the oscilloscope. The signal appearing on the oscilloscope may represent either absorption or dispersion depending upon whether the successive signals on the oscilloscope trace are symmetrical or anti-symmetrical. When a 30 cycle sine-sweep voltage was applied to the horizontal plates of the oscilloscope, two resonance curves appeared on the oscilloscope screen. Proper adjustment of the phase of the horizontal sweep voltage brought these two curves into coincidence. A Polaroid Land camera photographed the resonance curves directly from the oscilloscope.

For the case of broad and weak signals a lock-in amplifier was used with a 30 cycle modulating field of low amplitude. In order to provide a very slow sweep to run over the whole resonance line, a separate coil was mounted on one pole piece. The auxiliary coil supplied a small additional field parallel to the magnetic field, H_o. The direct current voltage of a few volts across the coil was varied slowly. In order to produce a voltage variation, a constant speed motor which changed the position of a rheostat contact was used.

The output of the lock-in amplifier is proportional to the slope of the resonance curve, and this output is connected to either a micro-ammeter or to a Millivac Sanborn chart recorder. From the recorder one obtains a trace of the derivative of the resonance curve. In this case the absorption component of the resonance is more generally used, and the width measured is the distance between the inflection points.

The samples used were heated by placing the sample coil inside a fiber tube through which hot air from an electric heater circulated. The voltage across the electric heater was controlled by a variac, and the rate of heating of the sample was quite uniform. The temperature of the sample was measured with a copper-constantan thermocouple placed directly in the sample. The maximum error in the measured temperature was about 1° C.

We shall now describe the experimental apparatus in more detail.

The Radio Frequency Bridge

The twin-T bridge described by Anderson[23] was used for all of the experimental work. A circuit diagram of the bridge is shown in Figure 4. The sample coil whose inside diameter is three-eighths inch and length five-eighths inch

23. H. L. Anderson, Phys. Rev. 76:1462 (1949).

consists of seven turns of No. 14 copper wire. The axis of the coil was perpendicular to the external magnetic field. One cubic centimeter of the compound which was being studied was placed in a glass test tube and the test tube was placed inside the coil. The coil is connected to the bridge by means of a coaxial line about ten inches long. The outer conductor of the line is a piece of brass tubing whose diameter is one-half inch. The brass tubing is grounded to the chassis of the bridge and the coil is connected to the tuning capacitor C, through the inner conductor of the coaxial line. The three series condensers C_1, C_2, and C'_1, are ceramic trimmers with a capacitance variable from five to ten $\mu\mu$f. The tuning condensers C and C' have a range from about 10 to 65 $\mu\mu$f. The trimmer on C consists of two brass discs. One disc is attached to a micrometer screw; and hence, a precise adjustment of the capacitance can be made. The trimmer on C' is a two-plate variable condenser, and a worm gear drive permits a slow variation of the capacitance.

One can balance the bridge by observing the oscilloscope pattern. Unless the bridge is balanced the trace remains smooth, but at balance the characteristic random noise appears on the screen. Adjustment of the field, H_o, to its proper value produces resonance.

The Phase-sensitive Amplifier and Thirty Cycle Generator

The circuit diagram of the tuned, phase-sensitive audio amplifier is shown in Figure 5. In this lock-in amplifier the twin-T filter stage, which is tuned for thirty cycles, passes a narrow band of harmonics; and hence, the noise is reduced, since the static field, H_o, is modulated by a 30-cycle alternating voltage applied to the modulating coils. A 30-cycle voltage from the generator is applied to the suppressor grids of the tubes V_3 and V_4, and the 30-cycle signal which is proportional to the derivative of the resonance line is applied to the control grid of the same tube. Consequently, the final result is both frequency and phase discrimination. The last stage is a balanced, direct-current amplifier. The generator which supplies the 30-cycle voltage is shown in Figure 6. The generator consists of a multivibrator and filters. A power amplifier provides the current for the modulation coils, and a phase-shifter circuit and amplification stage supplies the voltage for the suppressor grids of the phase-sensitive amplifier. The generator also provides the horizontal sweep-voltage of the oscilloscope.

The Electromagnet

The pole pieces of our magnet are six inches in diameter, and a central portion whose diameter is approximately three

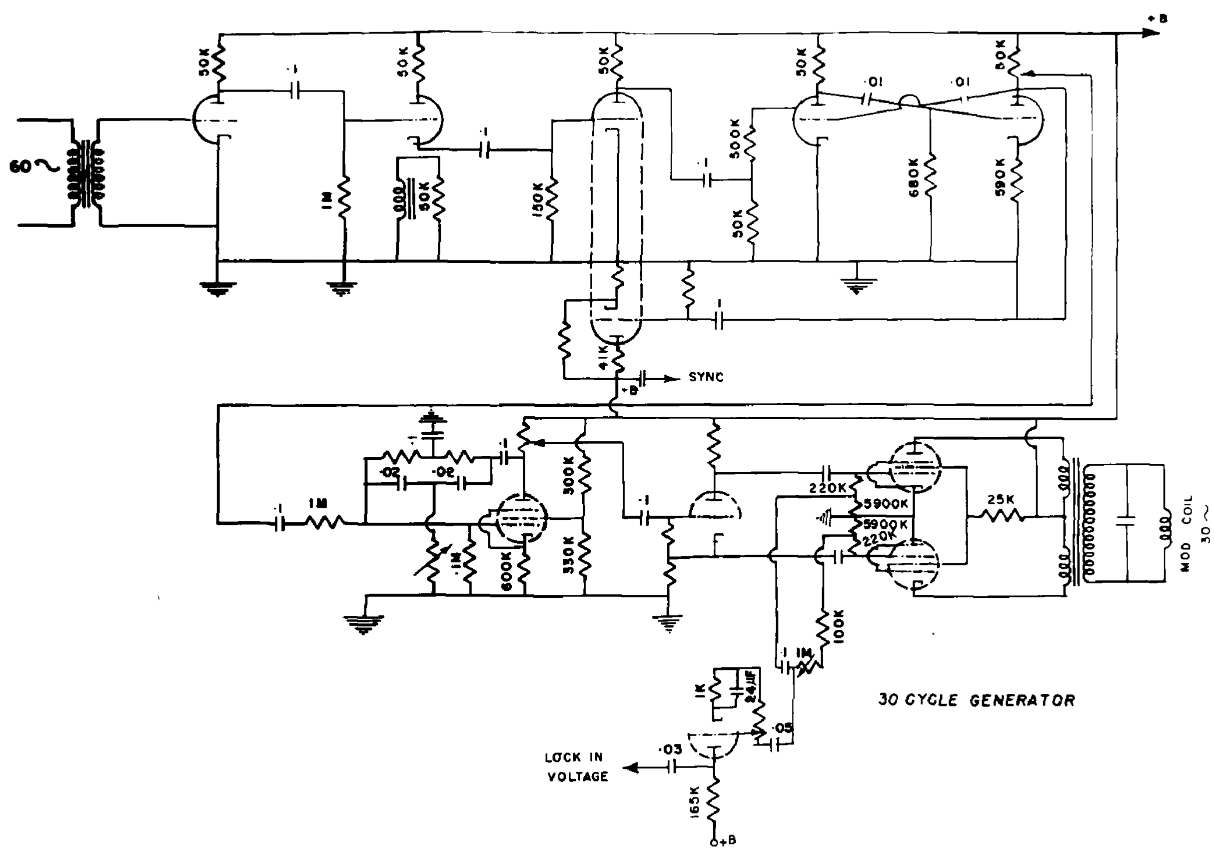

+B
60 ~
50K
·1
1M
50K
50K
150K
50K
SYNC
41K
+B
50K
·01
·01
50K
500K
50K
680K
590K
·02
·02
1M
·1M
600K
300K
330K
220K
5900K
5900K
220K
25K
100K
1M
1K
24µF
·05
·03
165K
+B
LOCK IN
VOLTAGE
MOD COIL
30 ~
30 CYCLE GENERATOR

Fig. 6.

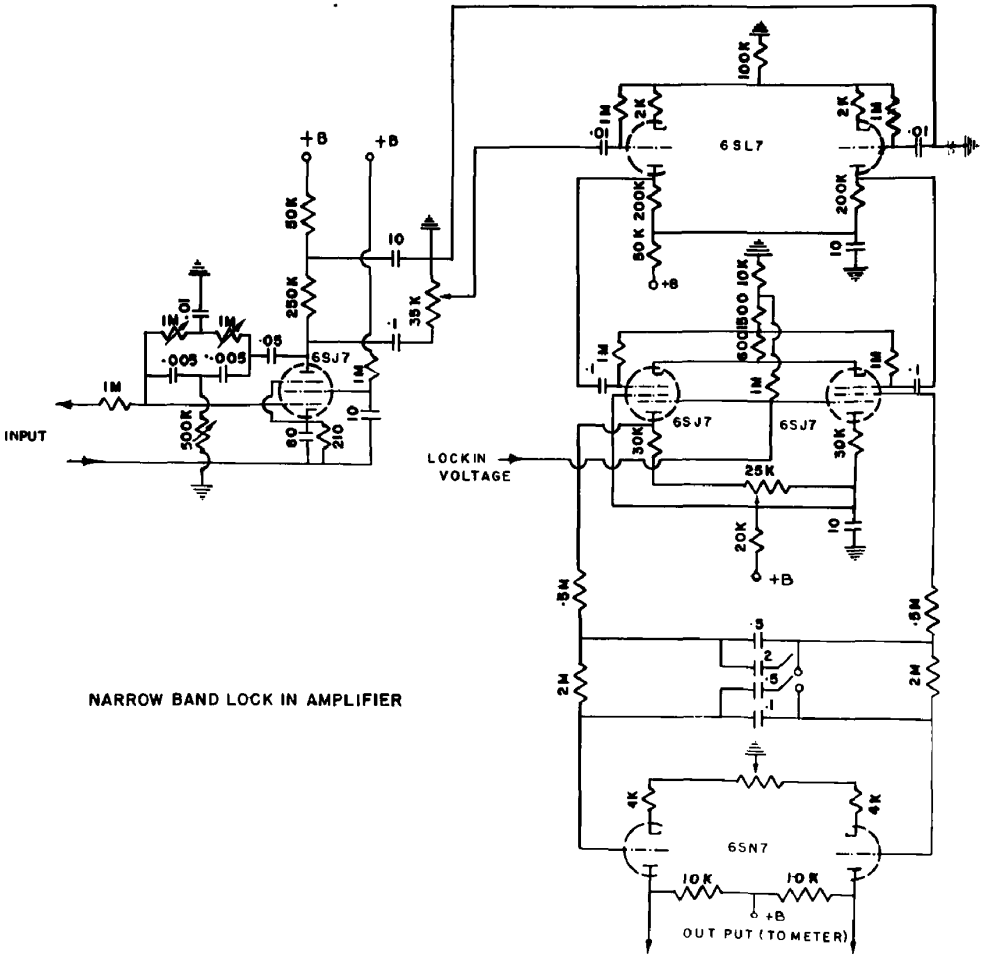

NARROW BAND LOCK IN AMPLIFIER

Fig. 5

inches, is flat within one-half a wave length of sodium light. The gap between the pole pieces was varied from one inch to two and one-half inches, but the maximum homogeneity of the field was obtained for a two-inch gap. Storage batteries with a capacity of 600 ampere-hours supplied the current for the magnet.

The normal operating field, 7300 gauss, required a current of 15 amperes; and the current was determined from the voltage drop across a small shunt resistor. The magnet was air cooled. The wire for the field coil was insulated with a coating of heavy Formex.

In order to obtain a more homogeneous magnetic field the pole pieces were simmed. The shims were made from "Delta-max", a ferro magnetic material. The "Delta-max" was soldered to brass pieces about two millimeters thick. These shims were moved about the faces of both pole pieces until the maximum homogeneity of the field was obtained.

In order to find the most homogeneous region of the magnetic field, the sample coil was moved about in the gap between the pole pieces. That region of the field in which the narrowest resonance line together with the maximum number of "wiggles" accompanied by an exponential decay appeared on the oscilloscope was considered the most homogeneous.

The "wiggles" phenomenon is a transient effect which

always appears after the sweep has passed through resonance. At resonance all the protons are in phase. The time lapse between successive wiggles varies as a function of the amplitude or the frequency of the sweep. The amplitude of these wiggles decays as the protons get out of phase with each other. The rate of decay of wiggles is given by[24]

$$e^{-\beta t(\Delta H + \delta H)}$$

where ΔH = line width in gauss

δH = inhomogeneity of the field over the volume of the sample

β = a constant for a given modulating field

t = time

One can measure either of two things from the decay. If δH, the inhomogeneity of the field, is small then one can neglect it; and the rate of decay measures the width of the line. On the other hand, if ΔH is small as compared with δH (e.g., distilled water where $\Delta H = 3 \times 10^{-3}$ gauss), the decay measures the inhomogeneity of the field over the volume of the sample. In our case the inhomogeneity, δH, is about .05 gauss over a sample whose volume is one cubic centimeter.

For a linear sweep, it has been shown[25] theoretically that in order to obtain a resonance line free of wiggles

---

24. Jacobson, Wangsness, Phys. Rev. 73:942 (1948).
25. Ibid., p. 942.

the relation $T_2 \left(\gamma \frac{d H_{mod}}{dt}\right)^{1/2}_{rms} \leq 1/2$ must be valid.

In this relation T_2 is the relaxation time;

γ is the gyromagnetic ratio; and

H_{mod} is the modulating field strength.

For the particular case of a Gaussian line shape

$$T_2 = \frac{2}{\gamma \Delta H} \quad . \tag{35}$$

Now $H_{mod} = H_m \sin \Omega t$,

where Ω is the angular frequency.

At the observation points

$$\frac{d H_{mod}}{dt} = \Omega H_m \, . \tag{36}$$

Here we are approximating the exact result

$$\Delta H = H_m \left(\Omega t - \frac{(\Omega t)^3}{24} + \frac{(\Omega t)^5}{480} - + \cdots\right) ,$$

by $\Delta H = \Omega H_m t$.

This approximation introduces an error of a few percent.

Hence, for no wiggles

$$H_m \leq \frac{1}{16} \frac{\gamma}{\Omega} (\Delta H)^2$$

$$\leq 0.706 (\Delta H)^2 \text{ for 60 cycles modulation}$$

$$\leq 1.41 (\Delta H)^2 \text{ for 30 cycles modulation.}$$

Calibration of the Modulating Field

In order to calibrate the modulating fields, we suppose that H_o is the d.c. value of the field and that the modulating a.c. field (H_m) is superimposed on H_o.

Suppose resonance occurs at the times (1) and (2) in Figure 7. Then from the Larmour frequency relation

$$\begin{aligned} \omega_1 &= \gamma (H_o + H_m) , \\ \omega_2 &= \gamma (H_o - H_m) , \\ \Delta\omega &= 2\gamma H_m , \\ H_m &= \frac{\Delta\omega}{2\gamma} \end{aligned} \qquad (37)$$

where ω = angular frequency

$\gamma = 4.257 \times 10^3$.

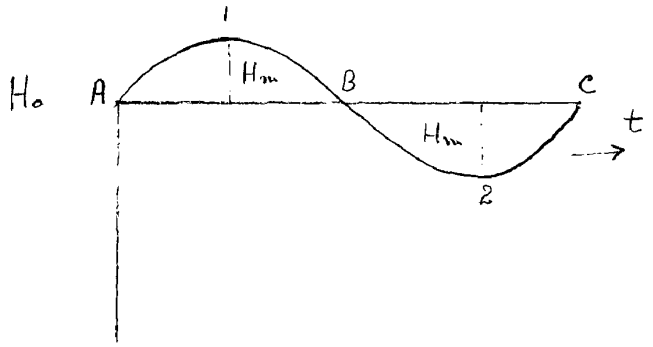

Figure 7. Total magnetic field plotted against time

When the signals are symmetrically placed they appear at the points A, B, C, etc. On increasing the frequency the signals at A and B move towards each other and ω_1 corresponds to the frequency when they both disappear at position

no. 1. Similarly on decreasing frequency, signals at B and C move towards each other and ω_2 corresponds to the frequency when they both disappear at the position no. 2. Then $\Delta\omega$ is the difference in the value of angular frequency in the two extreme cases. The magnitude of the modulating field strength, H_m depends upon the voltage applied to the modulating coils. A plot of field strength vs. voltage is a straight line except for voltages near zero.

Many factors contribute to the broadening of the resonance line. The modulating field can cause broadening unless the relation[26]

$$T_2\left(\gamma \frac{dH_{mod}}{dt}\right)^{1/2}_{res} \leq 1/5 \quad , \tag{38}$$

is valid. (Once again, this relation assumes a linear sweep). The symbols are explained in the previous section. For a Gaussian line shape

$$T_2 = \frac{2}{\gamma \Delta H} \quad ,$$

but $H_{mod} = H_m \sin \Omega t$.

Therefore, at the observation points

$$\frac{dH_{mod}}{dt} = \Omega H_m \quad ,$$

where we have made the same approximation as in the previous section. Hence, for a negligible broadening effect

$$H_m \leq \frac{1}{100} \frac{\gamma}{\Omega} (\Delta H)^2$$
$$\leq 0.113 (\Delta H)^2 \text{ for 60 cycle modulation}$$
$$\leq 0.226 (\Delta H)^2 \text{ for 30 cycle modulation.}$$

---

26. Ibid, p. 942.

Measurement of the Line Width

In order to measure the line width, let H_o be the value of d.c. field. The modulating field is superimposed on H_o as shown in Figure 8.

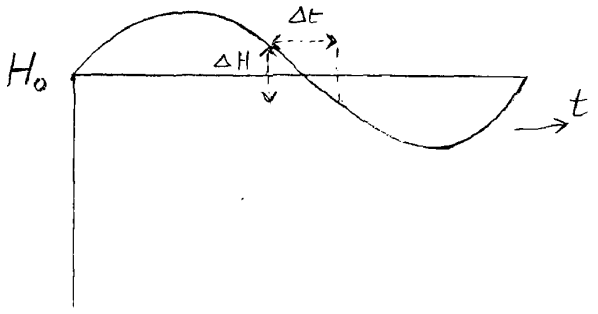

Figure 8. Total magnetic field plotted against time

The magnetic field at any point on this curve is given by the relation

$$H = H_o + H_m \sin \Omega t . \tag{39}$$

On differentiation one gets

$$dH = H_m \Omega \cos \Omega t \, dt .$$

If we change the frequency of the generator in such a way that we observe the signal near the zero of the sine curve, then

$$dH = H_m \Omega \, dt, \quad \text{or for small variation}$$

$$\Delta H = H_m \Omega \Delta t , \tag{40}$$

where Ω is the angular frequency of the modulating field; and Δt is the duration time for the line width. The quantity

Δt is obtained by recording with the resonance signal a time signal for a known frequency generated by a Hewlett Packard Audio Oscillator. Consequently, we were able to measure the width in gauss of the resonance line.

IV. RESULTS

Para-azoxyanisole 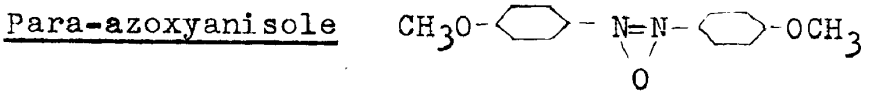

In the normal liquid phase of p-azoxyanisole, the proton resonance line is quite narrow and its apparent width is determined by the field inhomogeneity and the modulation effect. As the temperature is reduced below the clear point, i.e. the transition point between the liquid and the liquid crystal phase, p-azoxyanisole shows a first order transition at 135° C. The amplitude of the signal decreases greatly and the line splits into three components whose separation is somewhat greater than one gauss between the components. The line shape for p-azoxyanisole in liquid crystal phase is shown in Figure 9 and its derivative recorded with a Sanborn recorder is shown in Figure 10. The central line remains about 1.5 times as strong as the satellites throughout the liquid crystal phase with the intensity ratio of 2:3:2 among the three lines which is in good agreement with the areas under the maxima and also with the heights of these maxima. The behavior of the satellite separation with temperature in the range between the clear point (135° C.) and the solidification temperature (117° C.) is shown in Figure 11. The

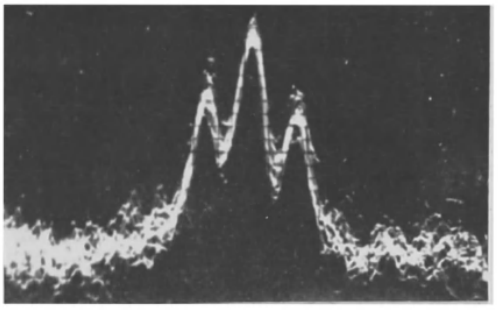

Fig. 9. Proton resonance line-shape of para-azoxyanisole in the liquid crystal phase.

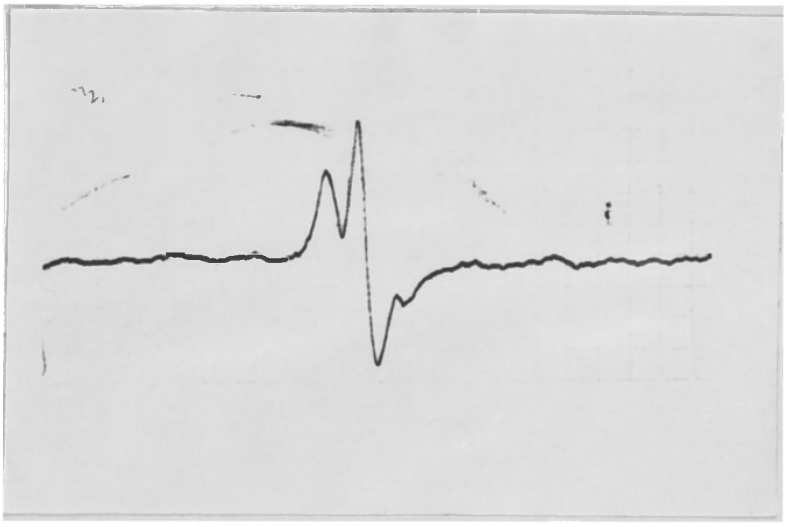

Fig. IO. Derivative of the resonance line for para--azoxyanisole in the liquid crystal phase.

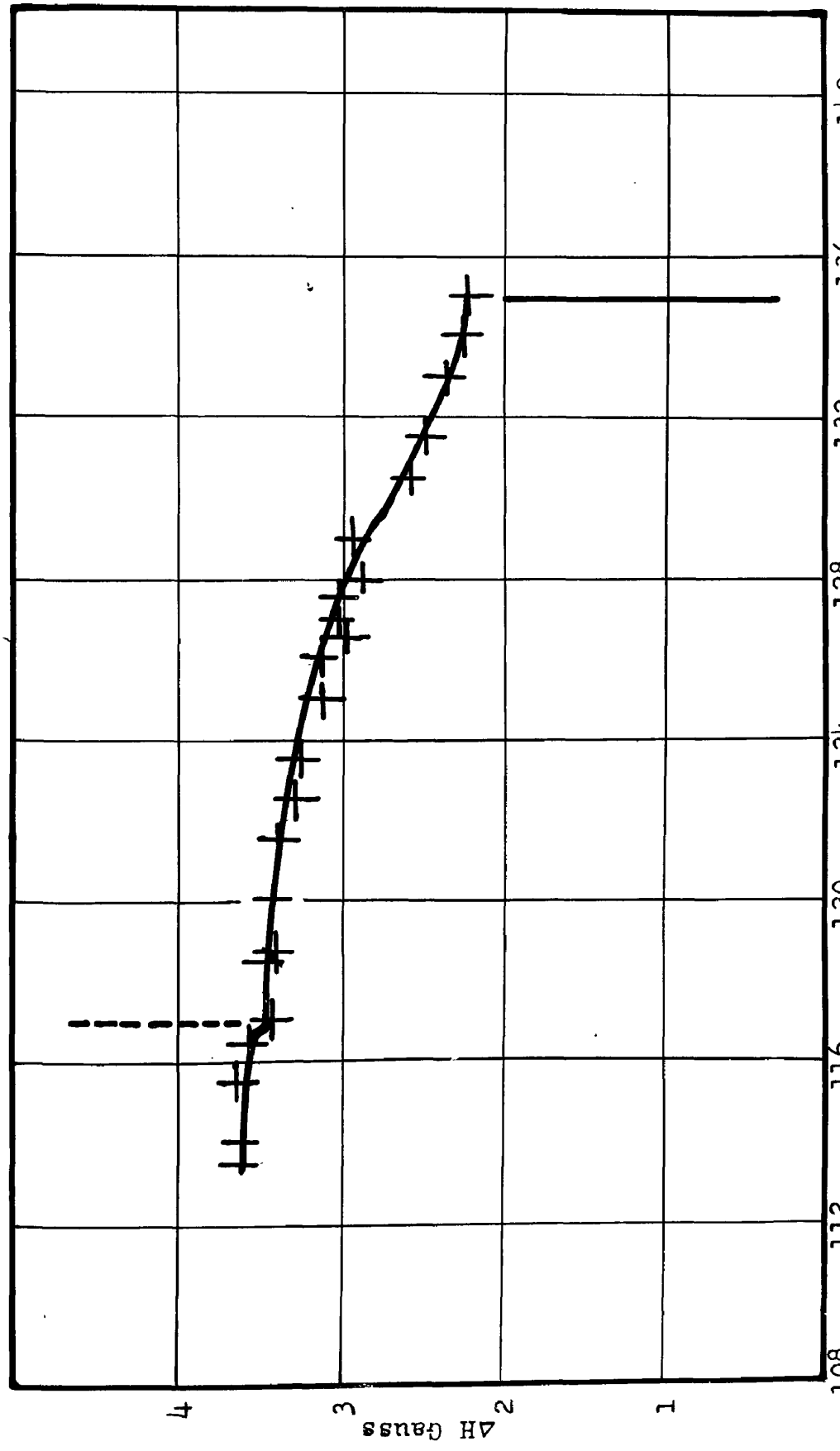

Figure 14. Peak to peak distance vs temperature for p-azoxyanisole [11]

error in determining the satellite separation at a given temperature arises primarily from our inability to read the peak positions accurately from our records and amounts to about ± .35 gauss. If the frequency of the modulating field is decreased to about 15 cycles/sec. the central line of the liquid crystal phase of p-azoxyanisole exhibits three closely spaced peaks at the top. With a little care the liquid crystal phase may be supercooled but the staellite separation in such a case remains at essentially the value at the solidification temperature. On passing into the solid state 117° C., the signal again decreases and the line spreads out to a half width of the order of 8 gauss with a probable error estimated at ± .5 gauss. In the solid state of p-azoxyanisole, the proton resonance line has a narrow central spike.

Para-azoxyphenetole 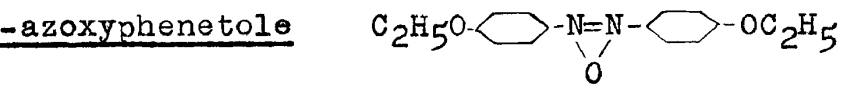

In the case of p-azoxyphenetole the line width in the normal liquid is very narrow as found in p-azoxyanisole. As the compound undergoes the transition at 166.6° C. from the liquid to the liquid crystal phase, the amplitude of the signal decreases considerably and the line splits into 3 components with the intensity ratio approximately 2:5:2 just near the transition temperature. But the central component shrinks down to the level of the satellite as the

temperature is reduced. At the lower temperature two additional small staellites appear near the central component, making a total of five components. This observation has been further checked by comparison with the differentiated line shape obtained from the lock-in amplifier and recorded with a Sanborn recorder and is shown in Figure 12. Successive stages in this process are shown at temperatures 166°, 165°, 159°, 144° and 140° C. in Figure 13 (a, b, c, d and e, respectively). The behavior of the separation of the outer satellite with temperature in the range between the clear point 166.6° C. and the solidification temperature 136° C. for the case of p-azoxyphenetole is shown in Figure 14. In this case the accuracy to which one can measure the position of the satellite is much poorer than in the case of p-azoxyanisole since the satellites grow progressively more poorly defined as the temperature is reduced. The line width in the solid state is about 7 gauss.

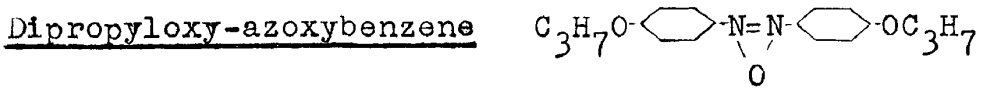

In the normal liquid phase of dipropyloxy-azoxybenzene the proton resonance line is quite narrow as in the case of p-azoxyanisole and p-azoxyphenetole. As the temperature is reduced below the clear point, it shows three lines. As this compound was considered to be impure, further investigation was not made.

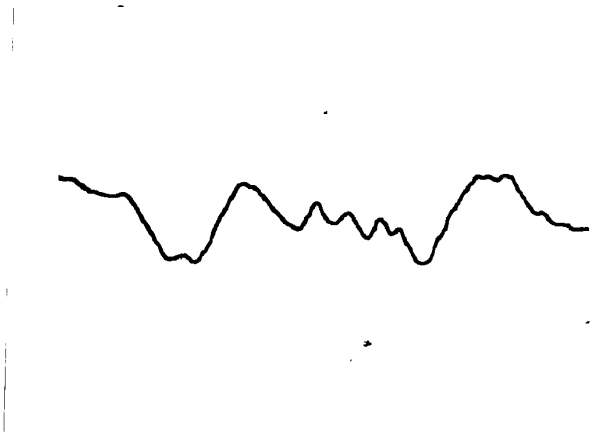

Fig. I2. Derivative of the resonance line of para-azoxyphenetole in the liquid crystal phase.

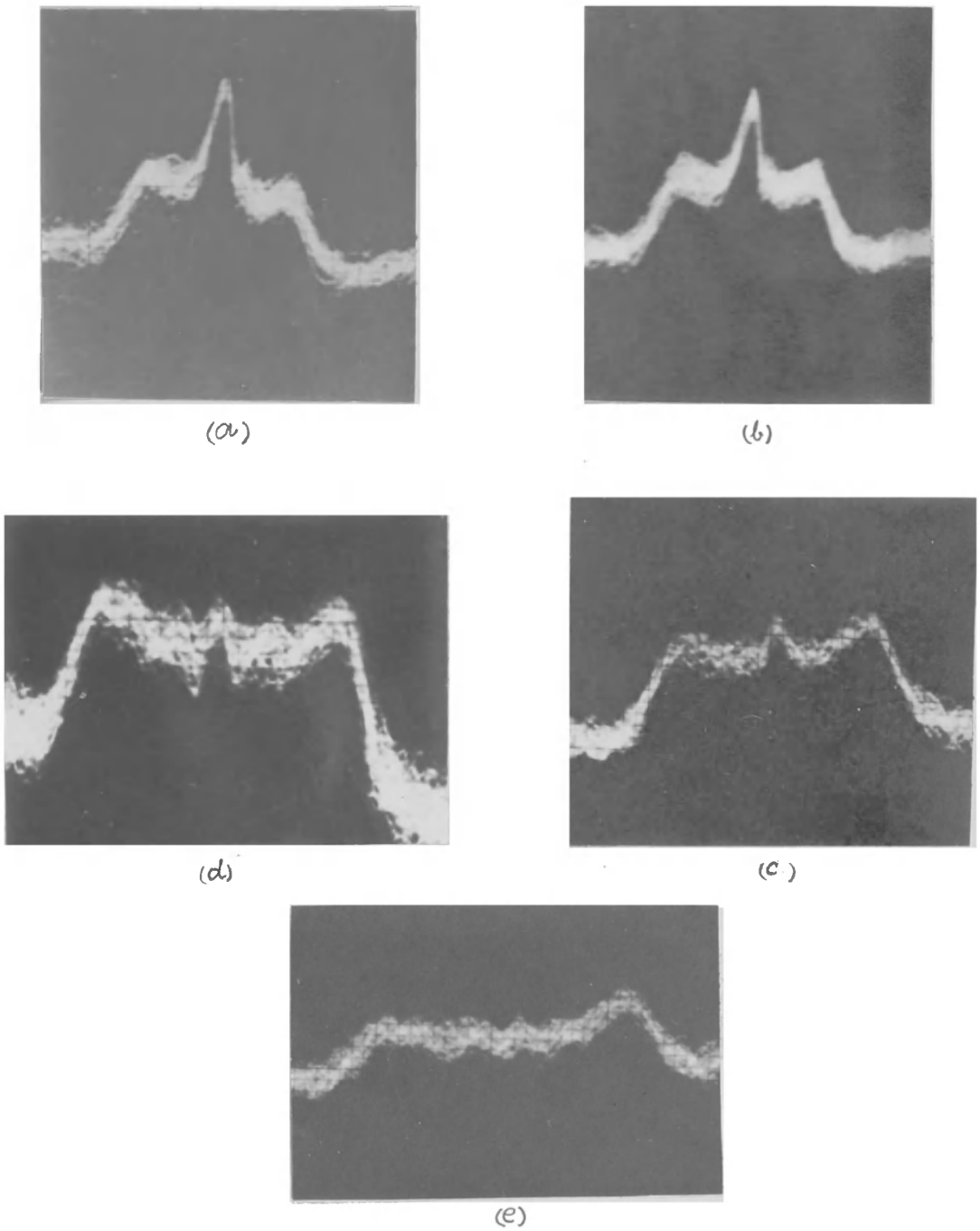

Fig. I3. Proton resonance line shape of para-azoxyphenetole in the liquid crystal phase at different temprature.

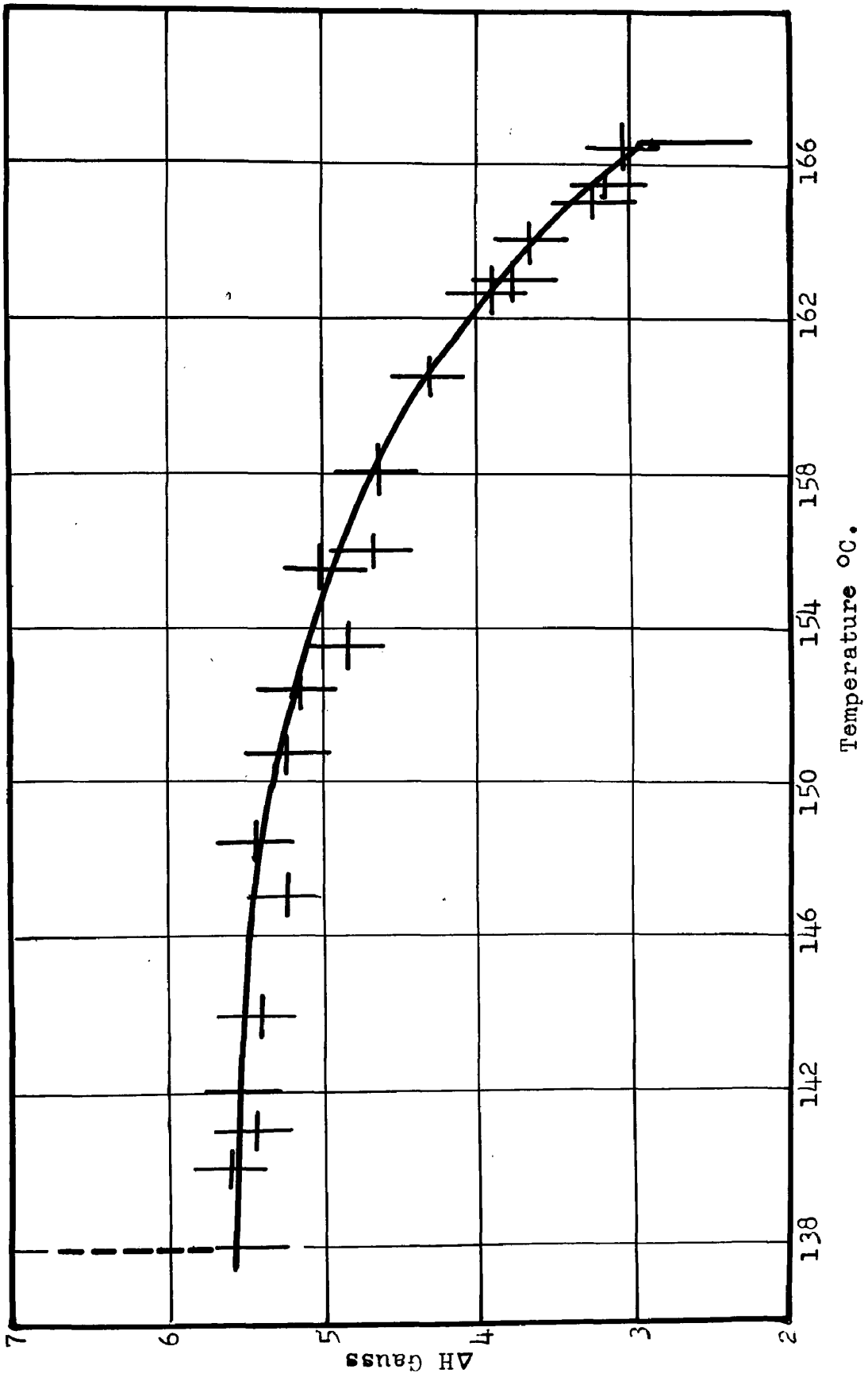

Figure 14. Peak to peak distance vs temperature for p-azoxyphenetole

V. DISCUSSION

The very interesting line shapes which appear in the liquid crystal phase of para-azoxyanisole and para-azoxyphenetole were found to be field independent in the small range of the fields available to us. This fact has been further verified by Dr. Gutowsky[27] and his colleagues at the University of Illinois. It therefore appears that the observed structure of the absorption lines is due to the magnetic dipolar interactions of the protons in these materials.

In order to calculate the lines from single molecules of para-azoxyanisole and para-azoxyphenetole, we consider the models of these compounds as shown in Figure 15.

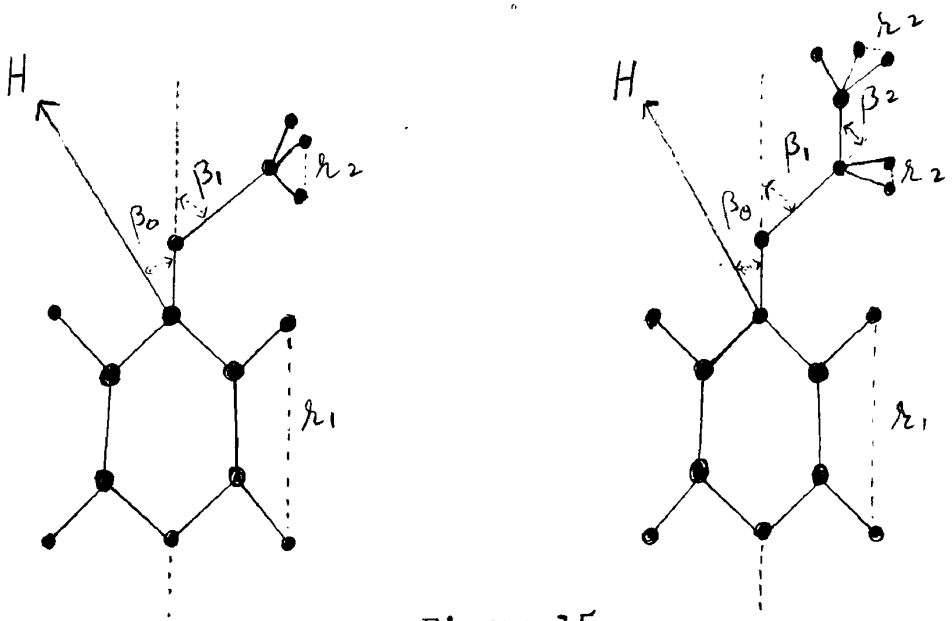

Figure 15

27. Spence, Gutowsky and Holm, J. Chem. Physics 21:1891 (1953).

In these models the following assumptions have been made:

a) Para-azoxyanisole

1. The protons in the CH_3 group lie in a plane perpendicular to O-C bond.
2. There is rotation about O-C and C-O bonds.
3. There is also rotation about the molecular axis, although this assumption is not essential.

b) Para-azoxyphenetole

1. The protons in the CH_3 group lie in a plane perpendicular to C-C bond.
2. The protons in the CH_2 group lie in a plane perpendicular to O-C bond.
3. There is rotation about C-C, O-C and C-O bonds.

The molecular constants used in the above models are:[28]

1. $r_1 = 2.45$ A°
2. $r_2 = 1.79$ A°
3. bond angles = 110°, $\beta_1 = \beta_2 = 70°$
4. β_o is the angle that the molecular axis makes with the direction of the magnetic field.

In order to find lines arising from dipole-dipole interaction for the case of a single molecule, we use the Eq. (11) in a more general form:[29]

$$H_i = H_o \pm \lambda_i (3 \cos^2 \beta_o - 1) \quad , \qquad (41a)$$

where constant λ_i has the following values:

---

28. Gordy, Microwave spectroscopy, John Wiley & Sons, (1953) p. 371.
29. Andrew and Bersohn, J. Chem. Physics 18:159 (1950).

1. Constants for para-azoxyanisole

$$\lambda_1 = \alpha_1 = 1.44 \text{ gauss} \qquad (41b)$$

$$\lambda_2 = \frac{\alpha_2}{2}(3\cos^2\beta_1 - 1) = 1.20 \text{ gauss}$$

where $\alpha_1 = \frac{3\mu}{2r_1^3} = 1.44$ gauss (for hydrogen of benzene group)

$$\alpha_2 = \frac{3\mu}{2r_2^3} = 3.69 \text{ gauss (for hydrogen of } CH_3 \text{ group)}$$

μ is proton magnetic moment and is equal to 2.79 nuclear magnetons or is equal to 14.09×10^{-24} gauss per cm^3.
w_i is the weight of each line which depends upon the number of protons representing that line and has the following values:

$$w_1 = \frac{4}{7} \times \frac{1}{2} = 0.286$$

$$w_2 = \frac{3}{7} \times \frac{1}{4} = 0.107$$

$$w_3 = \frac{3}{7} \times \frac{1}{2} = 0.214$$

such that $2w_1 + 2w_2 + w_3 = 1$

2. Similarly, the constants for para-azoxyphentole are:

$$\lambda_1 = \alpha_1 = 1.44 \text{ gauss}$$

$$\lambda_2 = \frac{\alpha_2}{4}(3\cos^2\beta_1 - 1) = 0.60 \text{ gauss}$$

$$\lambda_3 = \frac{\alpha_2}{4}(3\cos^2\beta_1 - 1)(3\cos^2\beta_2 - 1) = 0.39 \text{ gauss} \qquad (42)$$

$$\lambda_4 = 0 = 0 \text{ gauss}$$

The weight of each line is given by:

$$w_1 = \frac{4}{9} \times \frac{1}{2} = .222$$

$$w_2 = \frac{2}{9} \times \frac{1}{2} = .111$$

$$w_3 = \frac{3}{9} \times \frac{1}{4} = .083$$

$$w_4 = \frac{3}{9} \times \frac{1}{2} = .167$$

Line Shape for the Entire Sample

In order to find the line shape for the entire sample, one has to make some assumption about the orientation of the molecular axes with respect to the magnetic field. We shall consider the following possible assumptions as to the orientation of the molecular axes and shall discuss them in the order in which they are listed.

I. Complete orientation

II. Random orientation

III. Partial orientation

For the complete orientation of the molecular axes with the magnetic field β_0 will be zero, so that Eq. (40) becomes

$$H_i = H_0 \pm 2\lambda_i$$

and the separation between the pair of lines is given by

$$\delta H_i = 4\lambda_i \qquad (43)$$

For the case of para-azoxyanisole, the components of the

lines are separated as follows:

1. The hydrogens on the benzene ring give rise to a doublet whose components are separated by $\delta H_1 = 4\lambda_1 = 5.76$ gauss. The intensity of each line is given by $w_1 = 0.286$.
2. The hydrogens on the CH_3 group give rise to a triplet. The central line is surrounded by an equally spaced doublet separated by $\delta H_2 = 4\lambda_2 = 4.8$ gauss

The central line has an intensity $w_3 = 0.214$, while the two surrounding lines have their intensities each equal to $w_2 = 0.107$. The complete picture is shown in Figure 16.

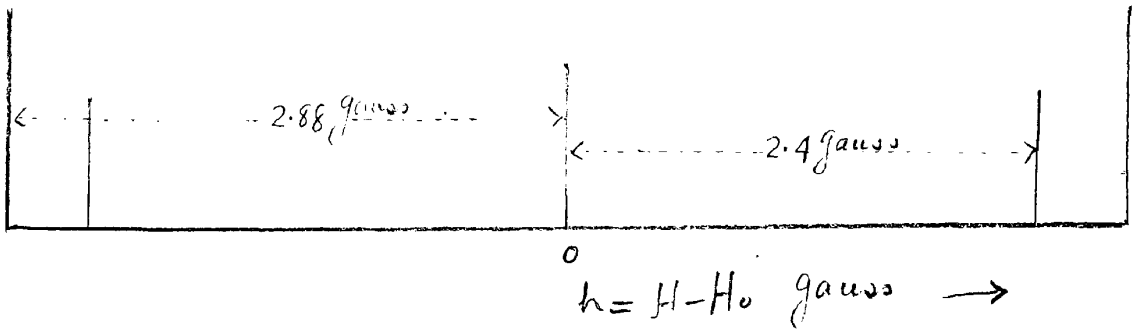

Figure 16

The components of the lines in the case of para-azoxyphentole are as follows:

1. The hydrogens on the benzene ring give rise to a doublet whose components are separated by

$\delta H_1 = 4\lambda_1 = 5.76$ gauss. Each of these lines has an intensity equal to $w_1 = 0.222$.

2. The hydrogen(s) on the CH_2 group give rise to a doublet separated by $\delta H_2 = 4\lambda_2 = 2.4$ gauss. Intensity of each line is equal to $w_2 = 0.111$.

The hydrogens on the CH_3 group give rise to a triplet. The central line is surrounded by an equally spaced doublet separated by $\delta H_3 = 4\lambda_3 = 1.56$ gauss. The central line has an intensity $w_4 = 0.167$, while each line of the doublet has an intensity $w_3 = 0.083$. The whole picture is shown in Figure 17.

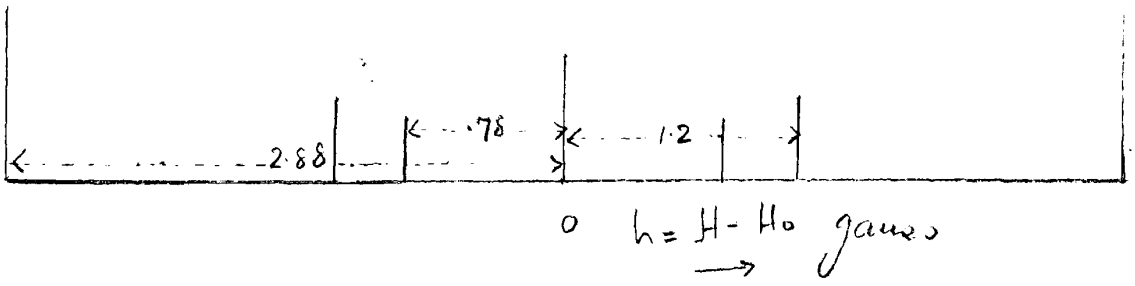

Figure 17

If the assumption of complete orientation were correct then the outer lines should be equally wide for both para-azoxyanisole and para-azoxyphenetole, and their spacing should be independent of temperature. However, our experimental

results show that neither of these two things is true. The outer lines of para-azoxyphenetole show a greater separation than para-azoxyanisole. Furthermore, the separation of the outer lines in para-azoxyanisole, as shown in Figure 16, is much wider than observed in our experiment. Moreover, there are only three lines observed throughout the liquid crystal range and not five as shown above. Similarly, in the case of para-azoxyphenetole there have been observed either three lines at high temperature or five lines at low temperature in the liquid crystal range and not seven as shown in Figure 17. On the whole the predictions based on the hypothesis of complete orientation of the molecules by the magnetic field are very different from the experimental results we have obtained. Consequently, we are forced to consider that our experiment shows that even in the large magnetic fields employed in our experiment, the orientation is not complete.

We next consider the case of random orientation of the molecular axes with the magnetic field. The orientation of the axes of a crystalline powder or an aggregate of swarms may be described by an isotropic distribution in angle. Such a distribution defines through Eq. (41a) (~~40~~), a distribution of resonance lines in the magnetic field. Since in Eq. (41a) (~~40~~) $(3\cos^2\beta_0-1)$ takes on all of its values in the range $\beta_0 = 0$ to $\beta_0 = \frac{\pi}{2}$, we write the angular distribution function over only this range of β_0 variation. The number of transitions

per unit time governed by the positive sign, N_+, is the same as that of those governed by the negative sign, N_-. Let N be the total number of transitions per unit time, and dN be the number of transitions arising from protons in crystallites whose axes lie in the solid angle $d\Omega$. Then

$$dN = N\frac{d\Omega}{4\pi} = -\frac{N}{2}\, d(\cos\beta_o)$$

But $dN_+ = dN_- = \frac{dN}{2}$

$$\therefore\quad dN_+ = -\frac{N}{4}\, d(\cos\beta_o) \tag{44}$$

From Eq. (40):

$$\cos\beta_o = \pm\frac{1}{\sqrt{3}}\left(1+\frac{h}{\lambda_i}\right)^{1/2} \qquad \text{when } -\lambda_i \le h \le 2\lambda_i \tag{45}$$

and $H_i - H_o \equiv h$

$$= \pm\frac{1}{\sqrt{3}}\left(1-\frac{h}{\lambda_i}\right)^{1/2} \qquad \text{when } -2\lambda_i \le h \le \lambda_i$$

Also, differentiating Eq. (40) one gets

$$dh_i = \pm 6\lambda_i \cos\beta_o\, d(\cos\beta_o) \tag{46}$$

From Eq. (44)

$$N_+ = \frac{N}{2}\int_{H_o+2\lambda_i}^{1} d(\cos\beta_o)$$

$$= \frac{N}{2}\int_{H_o-\lambda_i} P_+(h_i)\, dh_i \tag{46a}$$

where $P_+(h_i)\, dH_i$ is the probability that a transition for the positive sign in Eq. (40) occurs in a range dh_i.

Using Eq. (40), (41a) $d((\cos\beta_0))$ may be expressed in terms of and h_i , so that from Eq. (46a) we get

$$N_+ = \frac{N}{2}\int_{-\lambda_i}^{2\lambda_i} \frac{\sqrt{3}}{6\lambda_i}\,\frac{1}{\left(1+\frac{h}{\lambda_i}\right)^{1/2}}\,dh \quad ,$$

$$N_- = \frac{N}{2}\int_{-\lambda_i}^{2\lambda_i} \frac{\sqrt{3}}{6\lambda_i}\,\frac{1}{\left(1-\frac{h}{\lambda_i}\right)^{1/2}}\,dh \quad ;$$

The resultant total distribution function is given by

$$P(h) = \sum_{i=1}^{i=N} p_i(h)$$

where for the ith group

$$p_i(h) = \frac{\sqrt{3}}{6\lambda_i}\,\omega_i\left(1-\frac{h}{\lambda_i}\right)^{-1/2} \quad \ldots\ldots\ldots\ldots -2\lambda_i \le h \le -\lambda_i$$

where w_i is the intensity of ith line.

$$p_i(h) = \frac{\sqrt{3}}{6\lambda_i}\,\omega_i\left[\left(1-\frac{h}{\lambda_i}\right)^{-1/2} + \left(1+\frac{h}{\lambda_i}\right)^{1/2}\right] \quad \ldots\ldots -\lambda_i \le h \le \lambda_i$$

$$p_i(h) = \frac{\sqrt{3}}{6\lambda_i}\,\omega_i\left(1+\frac{h}{\lambda_i}\right)^{-1/2} \quad \ldots\ldots\ldots\ldots \lambda_i \le h \le 2\lambda_i \qquad (47)$$

$$p_N(h) = \omega_N\,\delta(0,h)$$

where w_N is intensity of the central line

The line shape P(h) calculated on the basis of the hypothesis

of random orientation of the axes of the swarms or crystallites in para-azoxyanisole is shown in Figure 18. In calculating the line shape of para-azoxyanisole the molecular constants given in section 1, Eq. (41) have been employed. The theoretical line shape for the case of para-azoxyphenetole is shown in Figure 19. This result is based on the molecular constants given in section 2, Eq. (42). Since the oscilloscope recording technique employed in this experiment yields the line shapes* without integration, the theoretical line shapes for para-azoxyanisole and para-azoxyphenetole given in Figures 18 and 19 may be directly compared with the corresponding experimental shapes given in Figures 9 and 10. If we do so, we notice in each case that the theoretical and experimental line shapes differ in width, but their structure exhibits some similarity apart from the extra discontinuities which are present in the calculated line shape. Such discontinuities in the theoretical line shape are smoothed out if we introduce the external broadening effect contributed by the neighboring molecules as well as from the different groups of the same molecule. We shall assume that the external broadening is of Gaussian type, although the use of only a Gaussian function is not rigorously justified, but is a simple approximation which indicates the broadening

*Actually a more sensitive comparison of line shapes could probably have been obtained by using a lock-in-amplifier which yields the derivative of the line shape and comparing such results with the derivative of the theoretical line shapes.

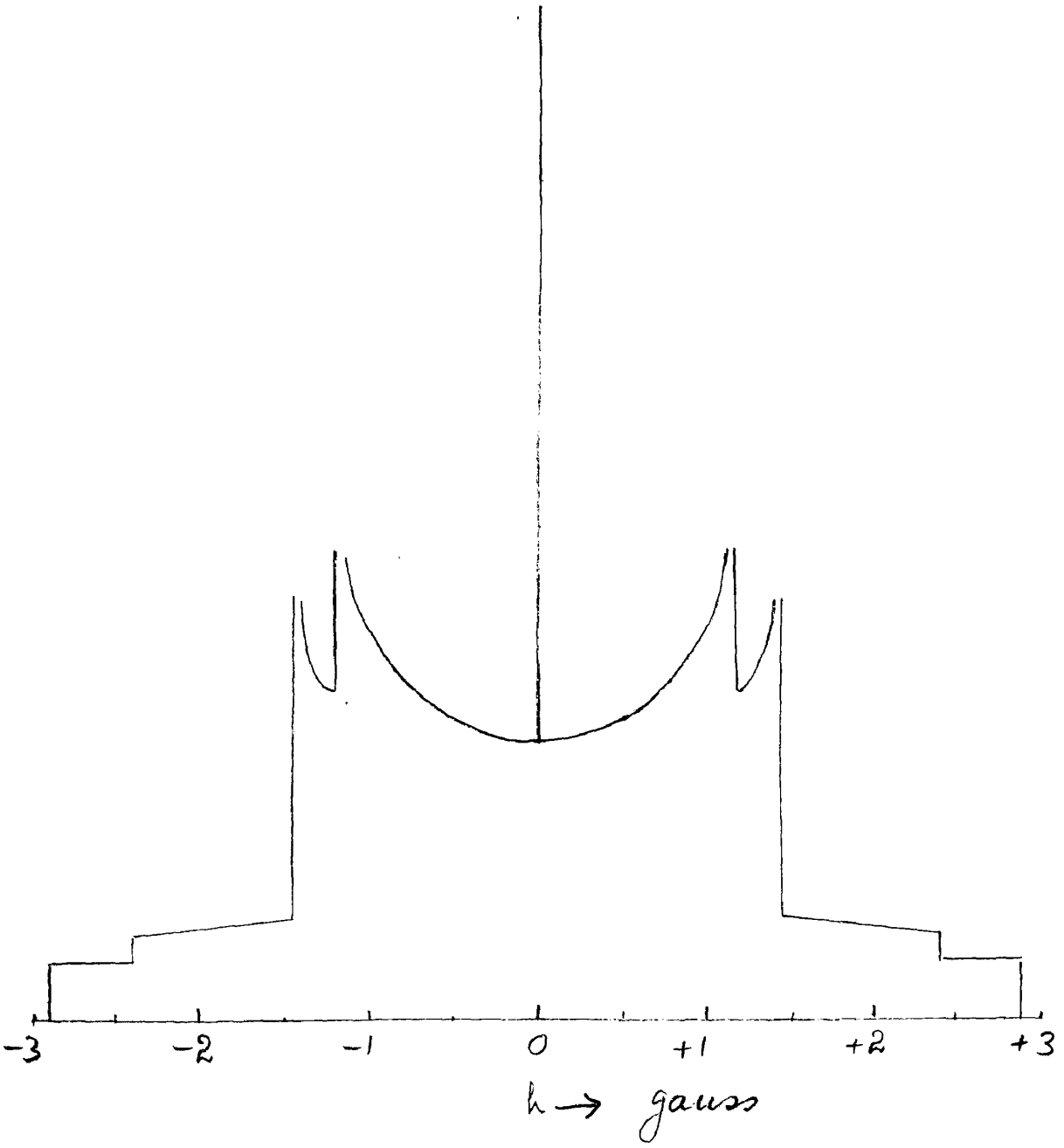

Figure 18. Para-azoxyanisole

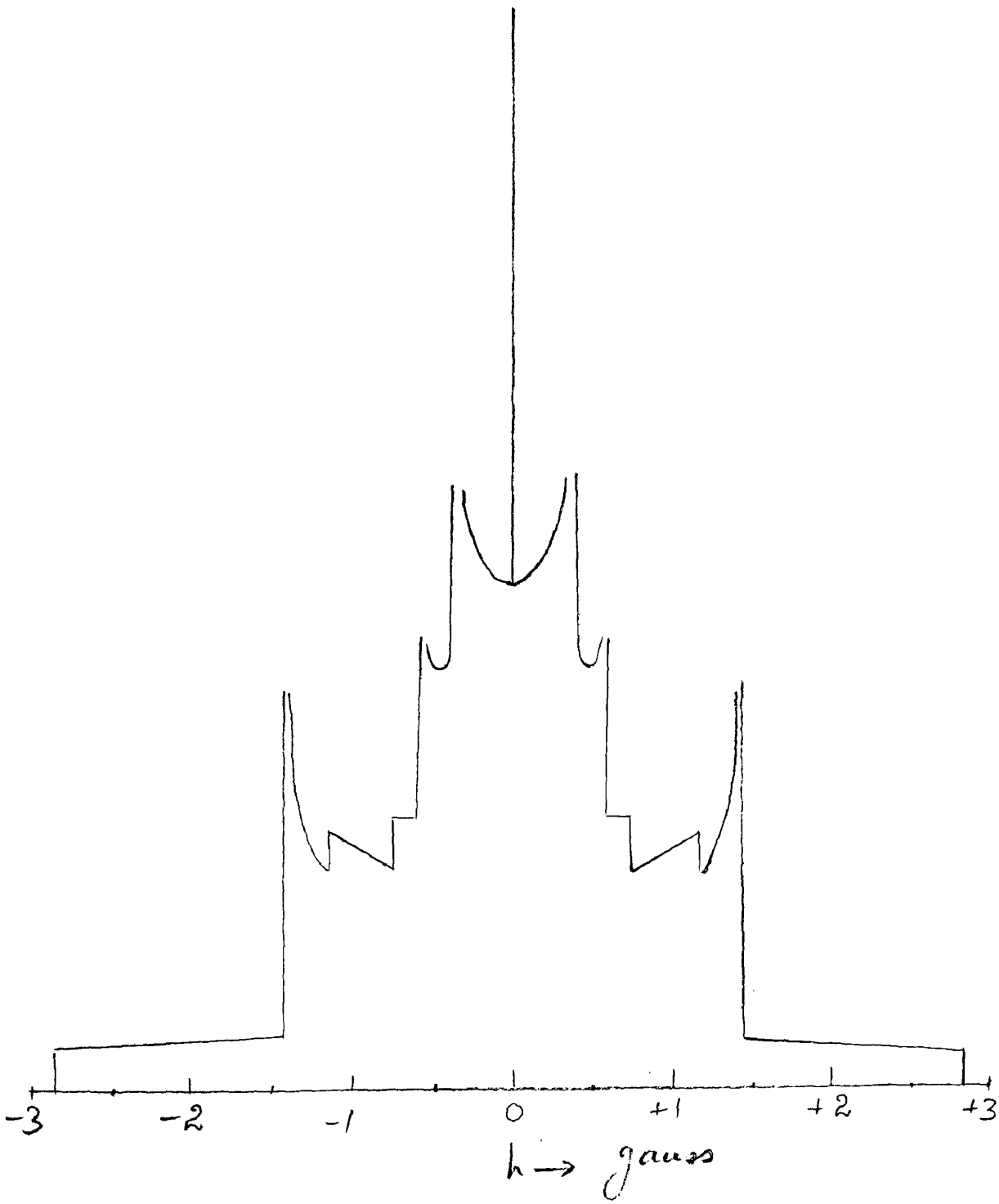

Figure 19. Para-azoxyphenetole

effect of neighboring groups.

If P'(h) is the resultant distribution function under the effect of Gaussian broadening, then

$$P'(h) = \sum_{i'=1}^{i=N} p_i'(h) \tag{48}$$

where $p_i'(h) = \int_{-\infty}^{\infty} g_i(h-h_1)\, p_i(h_1)\, dh_1$

and $g_i(h-h_1) = \frac{1}{\sqrt{2\pi}} \frac{1}{\sigma_i} e^{-\frac{(h-h_1)^2}{2\sigma_i^2}}$

where σ_i is the dispersion of the local fields at the ith group.

$$\therefore P'(h) = \sum_{i=1}^{i=N} \int_{-2\lambda_i}^{2\lambda_i} \frac{e^{-\frac{(h-h_1)^2}{2\sigma_i^2}}}{\sqrt{2\pi}\,\sigma_i} p_i(h_1)\, dh_1 \tag{49a}$$

$$P'(h) = \frac{w_N}{\sqrt{2\pi}} \frac{1}{\sigma_{N-1}} e^{-\frac{h^2}{2\sigma_{N-1}^2}} + \sum_{i=1}^{i=N-1} \frac{\sqrt{3}}{6\lambda_i} \frac{w_i}{\sqrt{2\pi}\,\sigma_i} \left[\int_{-2\lambda_i}^{2\lambda_i} \frac{e^{-\frac{(h-h_1)^2}{2\sigma_i^2}}}{\sqrt{1-\frac{h_1}{\lambda_i}}} dh_1 \right.$$

$$\left. + \int_{-\lambda_i}^{2\lambda_i} \frac{e^{-\frac{(h-h_1)^2}{2\sigma_i^2}}}{\sqrt{1+\frac{h_1}{\lambda_i}}} dh_1 \right] \tag{49b}$$

This may be written as

$$P'(h) = \frac{w_N}{\sqrt{2\pi}\,\sigma_{N-1}} e^{-\frac{h^2}{2\sigma_{N-1}^2}} + \sum_{i=1}^{i=N-1} \frac{w_i}{\sqrt{6}\,\lambda_i} \left\{ \frac{1}{\sqrt{2\pi}} \frac{1}{\alpha_i} \left[\int_0^3 \frac{e^{-\frac{(t_i'-t_i)^2}{\alpha_i^2}}}{\sqrt{t_i'}} dt_i' \right.\right.$$

$$\left.\left. + \int_0^3 \frac{e^{-\frac{(s_i'-s_i)^2}{\alpha_i^2}}}{\sqrt{s_i'}} ds_i' \right] \right\}.$$

where

$$\alpha_i^2 = \frac{2\sigma_i^2}{\lambda_i^2}$$

and

$$t_i' = 1 - \frac{h_1}{\lambda_i} \quad ; \quad S_i' = 1 + \frac{h_1}{\lambda_i}$$
$$t_i = 1 - \frac{h}{\lambda_i} \quad ; \quad S_i = 1 + \frac{h}{\lambda_i}$$

Now we set

$$G(x,\alpha) \equiv \frac{1}{\sqrt{2\pi}\,\alpha} \int_0^3 \frac{e^{-\frac{(x-y)^2}{\alpha^2}}}{\sqrt{y}}\, dy$$

then

$$P'(h) = \frac{\omega_N}{\sqrt{2\pi}} \frac{e^{-\frac{h^2}{2\sigma_{N-1}^2}}}{\sigma_{N-1}} + \sum_{i=1}^{i=N-1} \frac{\omega_i}{\sqrt{6}\,\lambda_i} \left\{ G\left((1-\tfrac{h}{\lambda_i});\alpha_i\right) + G\left((1+\tfrac{h}{\lambda_i});\alpha_i\right) \right\} . \tag{50}$$

Now the problem consists of the calculation of the integrals,

$$G(x,\alpha) \equiv \frac{1}{\sqrt{2\pi}} \frac{1}{\alpha} \int_0^3 \frac{e^{-\frac{(x-y)^2}{\alpha^2}}}{\sqrt{y}}\, dy \tag{51}$$

Let $\frac{x}{\alpha} = \varrho$ and $\frac{y}{\alpha} = \eta$

$$G((\alpha\varrho);\alpha) = \frac{1}{\sqrt{2\pi}} \frac{1}{\sqrt{\alpha}} \int_0^{3/\alpha} \frac{e^{-(\varrho-\eta)^2}}{\sqrt{\eta}}\, d\eta .$$

Let $z = \eta - \varrho$

$$G((\alpha\varrho);\alpha) = \frac{1}{\sqrt{2\pi}} \frac{1}{\sqrt{\alpha}} \int_{-\varrho}^{3/\alpha - \varrho} \frac{e^{-z^2}}{\sqrt{z+\varrho}}\, dz . \tag{52}$$

Now if $\varrho \gg 0$, the main contribution to the integrand comes

from around Z = 0, we may expand the radical about Z = 0 to calculate the integral.

Now since e^{-Z^2} is equal to 0.007 when $Z = \sqrt{5}$, we may replace the limits with $+\infty$ and $-\infty$ if $3/\alpha - \eta > \sqrt{5}$

$$\eta > \sqrt{5}$$

or if $$\sqrt{5} \leq \eta_1 \leq \frac{3}{\alpha} - \sqrt{5}$$

then

$$G((\alpha\eta);\alpha) = \frac{1}{\sqrt{2\pi}} \frac{1}{\sqrt{\alpha\eta}} \int_{-\infty}^{\infty} \left(1 - \frac{1}{8}(Z/\eta) + \frac{3}{8}(Z/\eta)^2 - \left(\frac{15}{48}\right)(Z/\eta)^3 + \frac{105}{384}\left(\frac{Z}{5}\right)^4 \cdots\cdots\right) e^{-Z^2} dZ$$

thus

$$G((\alpha\eta);\alpha) = \frac{1}{\sqrt{2}} \frac{1}{\sqrt{\alpha\eta}} \left(1 + \frac{3}{16}\left(\frac{1}{\eta}\right)^2 + \frac{105}{512}\left(\frac{1}{\eta}\right)^4 + \cdots\right)$$

since $X = \alpha\eta$ and $\eta = X/\alpha$

$$G(X,\alpha) = \frac{1}{\sqrt{2}} \frac{1}{\sqrt{X}} \left(1 + \frac{3}{16}\left(\frac{\alpha}{X}\right)^2 + \frac{105}{512}\left(\frac{\alpha}{X}\right)^4 + \cdots\right) \quad (53)$$

if $$\sqrt{5}\,\alpha \leq X \leq 3 - (\sqrt{5}\,\alpha)$$

We next consider the case $\eta = 3/\alpha + \epsilon$

where $|\epsilon| \leq 3/\alpha$

If $3/\alpha > \sqrt{5}$ we may take the lower limit = $-\infty$

$$G((\alpha\eta);\alpha) = \frac{1}{\sqrt{2\pi}} \frac{1}{\sqrt{\alpha}} \int_{-\infty}^{-\epsilon} \frac{e^{-Z^2}}{\sqrt{\left(\frac{3}{\alpha} + \epsilon\right) + Z}} dZ$$

$$= \frac{1}{\sqrt{2\pi}} \frac{1}{\sqrt{3+\alpha\epsilon}} \int_{-\infty}^{-\epsilon} \left\{ 1 - \frac{1}{2} \left(\frac{z}{(3/\alpha + \epsilon)} + \cdots \right) \right\} e^{-z^2} dz$$

$$\int_{-\infty}^{-\epsilon} e^{-z^2} dz = \int_{\epsilon}^{\infty} e^{-z^2} dz = \int_{0}^{\infty} e^{-z^2} dz - \int_{0}^{\epsilon} e^{-z^2} dz \qquad (54)$$

$$= \frac{\sqrt{\pi}}{2} \left(1 - P(\epsilon) \right).$$

where $P(\epsilon) = \frac{2}{\sqrt{\pi}} \int_{0}^{\epsilon} e^{-z^2} dz$ (30)

$$\int_{-\infty}^{-\epsilon} z\, e^{-z^2} dz = -\frac{1}{2} \int_{\epsilon^2}^{\infty} e^{-\eta} d\eta = -\frac{e^{-z^2}}{2}$$

$$\therefore \; G((\alpha\varrho); \alpha) = \frac{1}{\sqrt{2}} \frac{1}{2} \frac{1}{\sqrt{3+\alpha\epsilon}} \left\{ 1 - P(\epsilon) + \frac{e^{-\epsilon^2}}{2\sqrt{\pi}\left(3/\alpha + \epsilon\right)} \right\}$$

$$X = \alpha\varrho \quad \text{and} \quad \epsilon = \frac{X-3}{\alpha}$$

$$G(X, \alpha) = \frac{1}{\sqrt{2}} \frac{1}{2} \frac{1}{\sqrt{X}} \left\{ 1 - P\left(\frac{X-3}{\alpha}\right) + \frac{\alpha}{2\sqrt{\pi}} \frac{e^{-\left(\frac{X-3}{\alpha}\right)^2}}{X} \right\} \qquad (55)$$

Also $P(-Y) = -P(Y)$

If $\varrho \simeq 0$ none of the previous methods work. If $3/\alpha > \sqrt{5}$, we may take the upper limit as $+\infty$ and write

---

30. B. O. Peirce, A short table of integrals, Ginn and Company, (1910), p. 116.

$$G((\alpha\varphi);\alpha) = \frac{1}{\sqrt{2\pi}} \frac{1}{\sqrt{\alpha}} F(\varphi) \tag{56}$$

where $F(\varphi) = \int_0^\infty \frac{e^{-(\varphi-\eta)^2}}{\sqrt{\eta}}\, d\eta$

We set

$$F(\varphi) = \int_0^{\frac{1}{4}} \frac{e^{-(\varphi-\eta)^2}}{\sqrt{\eta}}\, d\eta + \int_{\frac{1}{4}}^\infty \frac{e^{-(\varphi-\eta)^2}}{\sqrt{\eta}}\, d\eta \tag{57}$$

$$\int_0^{\frac{1}{4}} \frac{e^{-(\varphi-\eta)^2}}{\sqrt{\eta}}\, d\eta = e^{-\varphi^2}\left[1 + \frac{1}{6}\varphi + \frac{(2\varphi^2-1)}{80} + \frac{(2\varphi^2-3\varphi)}{672} + \frac{4\varphi^4-12\varphi^2+3}{13,824} + \cdots\right] \tag{58}$$

$\int_{\frac{1}{4}}^\infty \frac{e^{-(\varphi-\eta)^2}}{\sqrt{\eta}}\, d\eta$ may be computed numerically. Results for F(G) are:

G	F(G)
- 1.5	0.100
- 1.0	0.409
- 0.5	1.051
+ 0	1.807
+ 0.5	2.12
+ 1.0	1.949
+ 1.5	1.595
+ 2	1.299
+ 3	1.038
+ 4	0.8925
+ 5	0.7895

With the help of Eqs. (53), (55) and (56), the function $G(x, \alpha)$ was calculated for different values of α, i.e., α = 0.10, 0.15, 0.20, 0.30 and 0.40. The results are shown in Figure 20. Thus, from Eq. (50) line shape P'(h) has been calculated for different values of the external broadening factor σ for the case of para-azoxyanisole and para-azoxyphenetole and are shown in Figures 21 to 26. In these plots α_i has been considered to be the same for all groups of the molecule. This procedure may be justified roughly as follows: In the expression

$$\alpha_i = \frac{\sqrt{2}}{\lambda_i} \sigma_i$$

λ_i decreases as the number of axes about which the ith group is rotating is increased. On the other hand, σ_i represents the dispersion of the local field experienced by the protons in the ith group and should also decrease as the number of axes of rotation is increased. Therefore α_i should remain approximately constant for all groups.

For the case of para-azoxyanisole, the following values of σ_i have been used for different groups of the molecules from the relation $\alpha_i^2 = \frac{2\sigma_i^2}{\lambda_i^2}$

Para-azoxyanisole

(1) For α_i = 0.1

σ_1 = 0.102 gauss

σ_2 = 0.085 gauss

(2) For α_i = 0.2

Figure 20

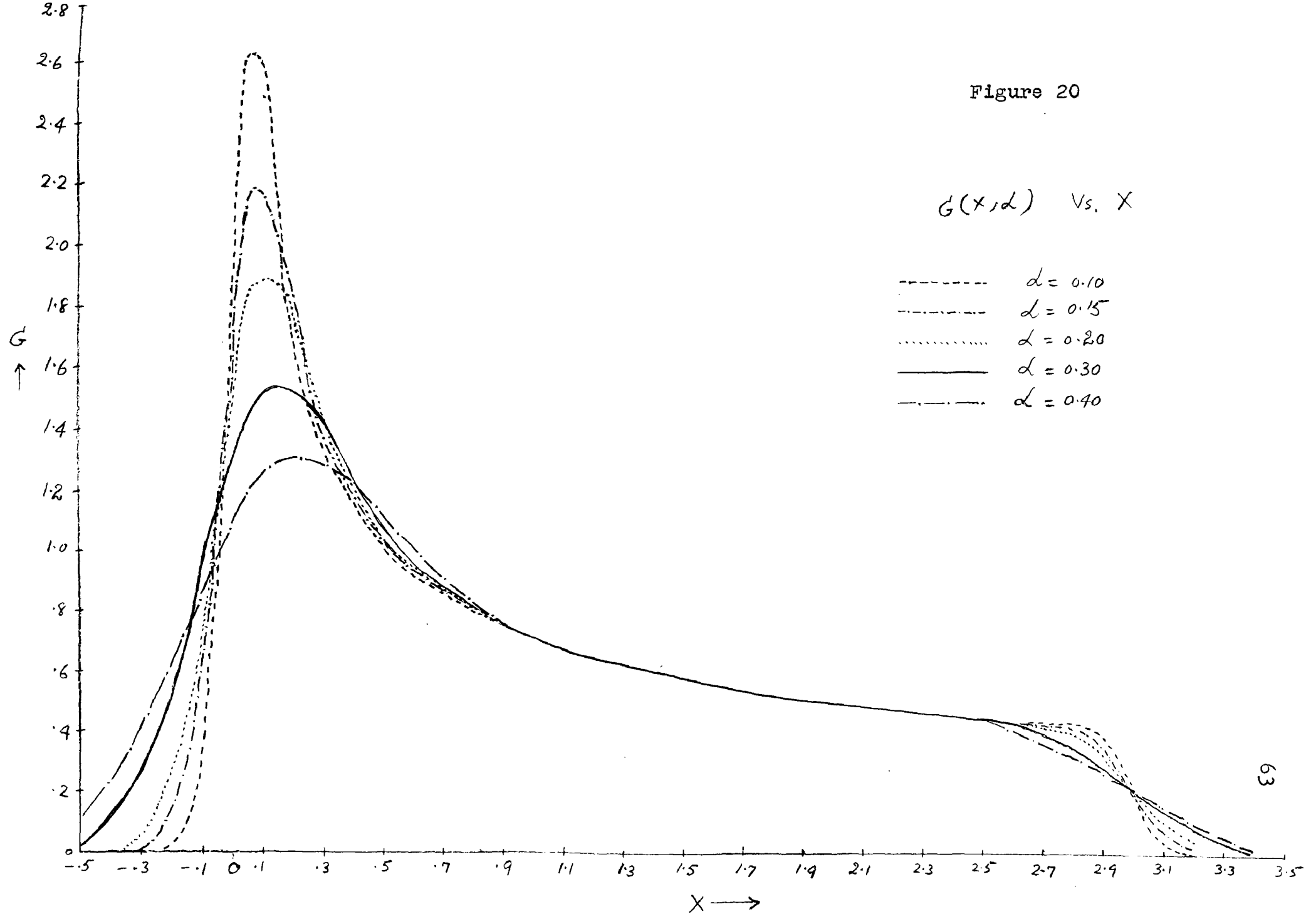
G(x,α) Vs. X
α = 0.10
α = 0.15
α = 0.20
α = 0.30
α = 0.40
G
X
2·8
2·6
2·4
2·2
2·0
1·8
1·6
1·4
1·2
1·0
·8
·6
·4
·2
0
-·5
-·3
-·1
0
·1
·3
·5
·7
·9
1·1
1·3
1·5
1·7
1·9
2·1
2·3
2·5
2·7
2·9
3·1
3·3
3·5

Figure 21

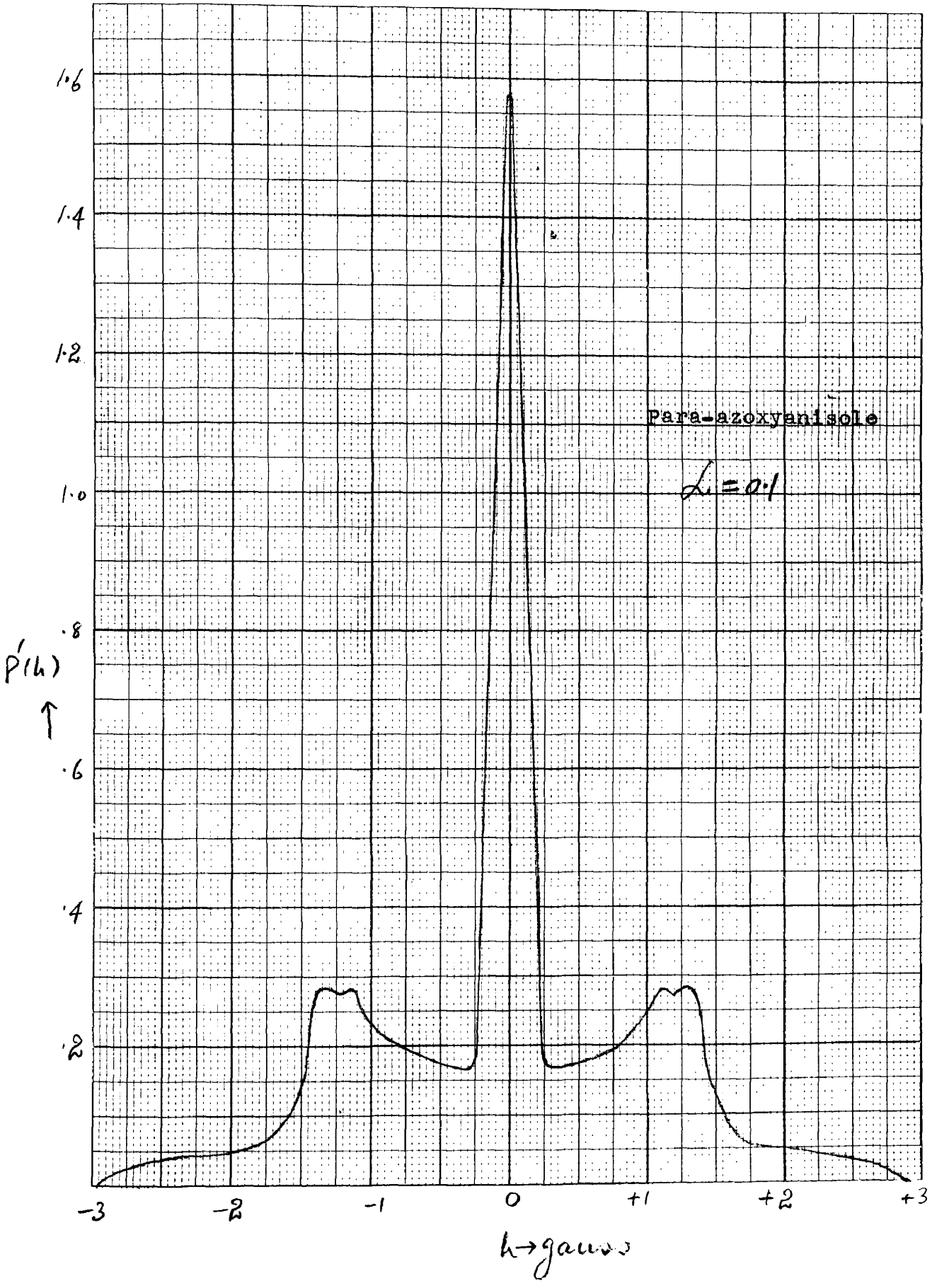

Figure 22

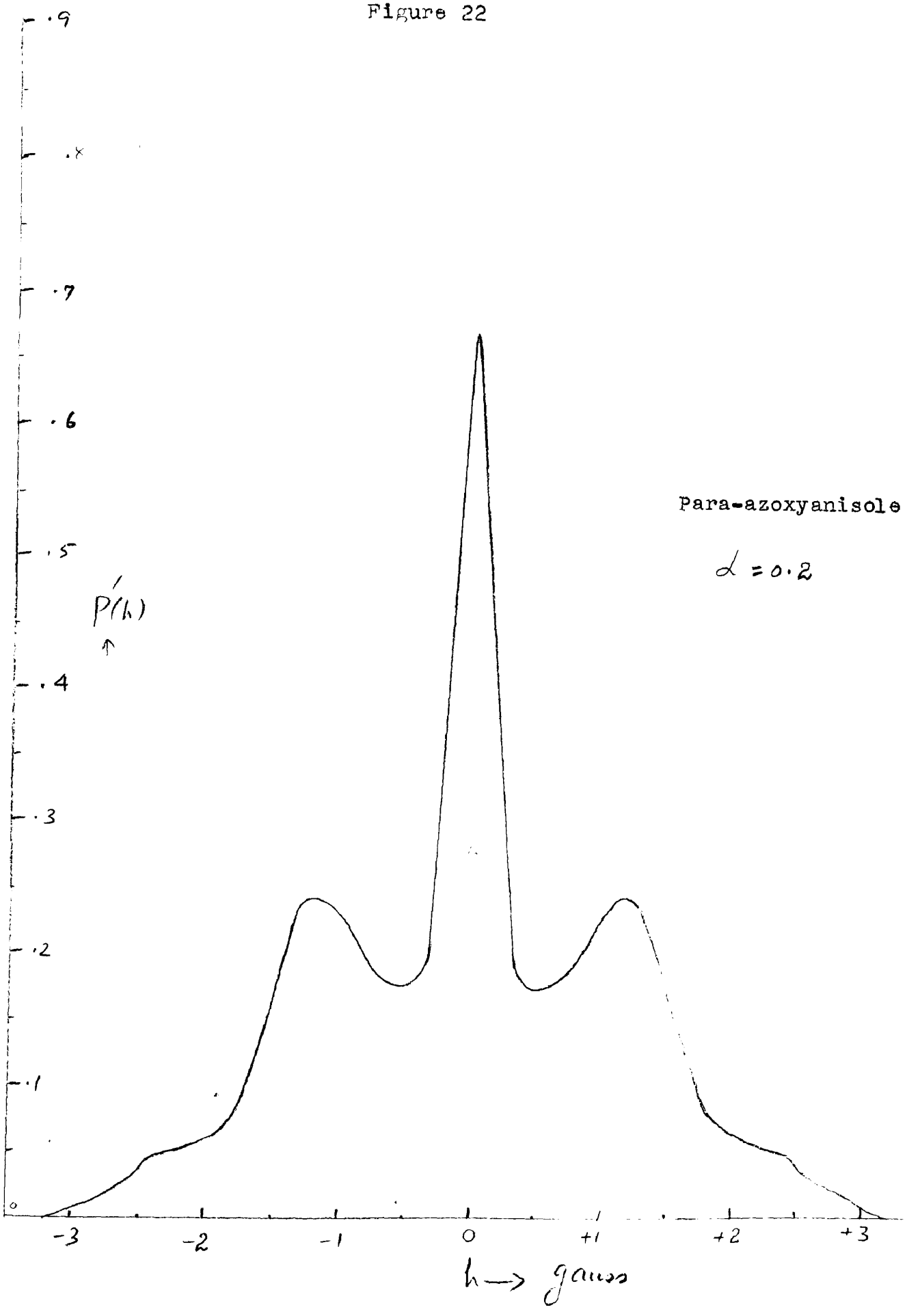

Figure 23

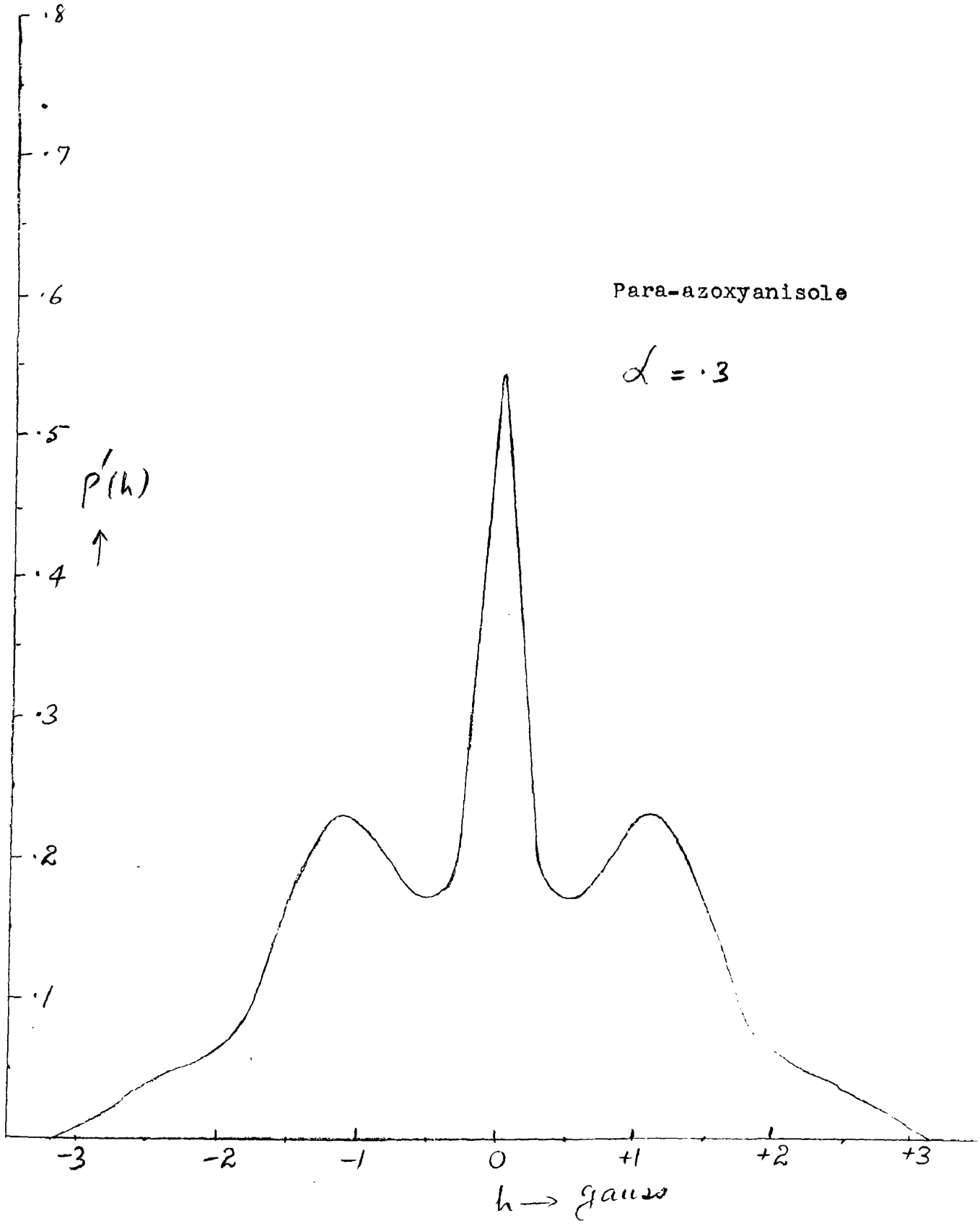

Figure 24

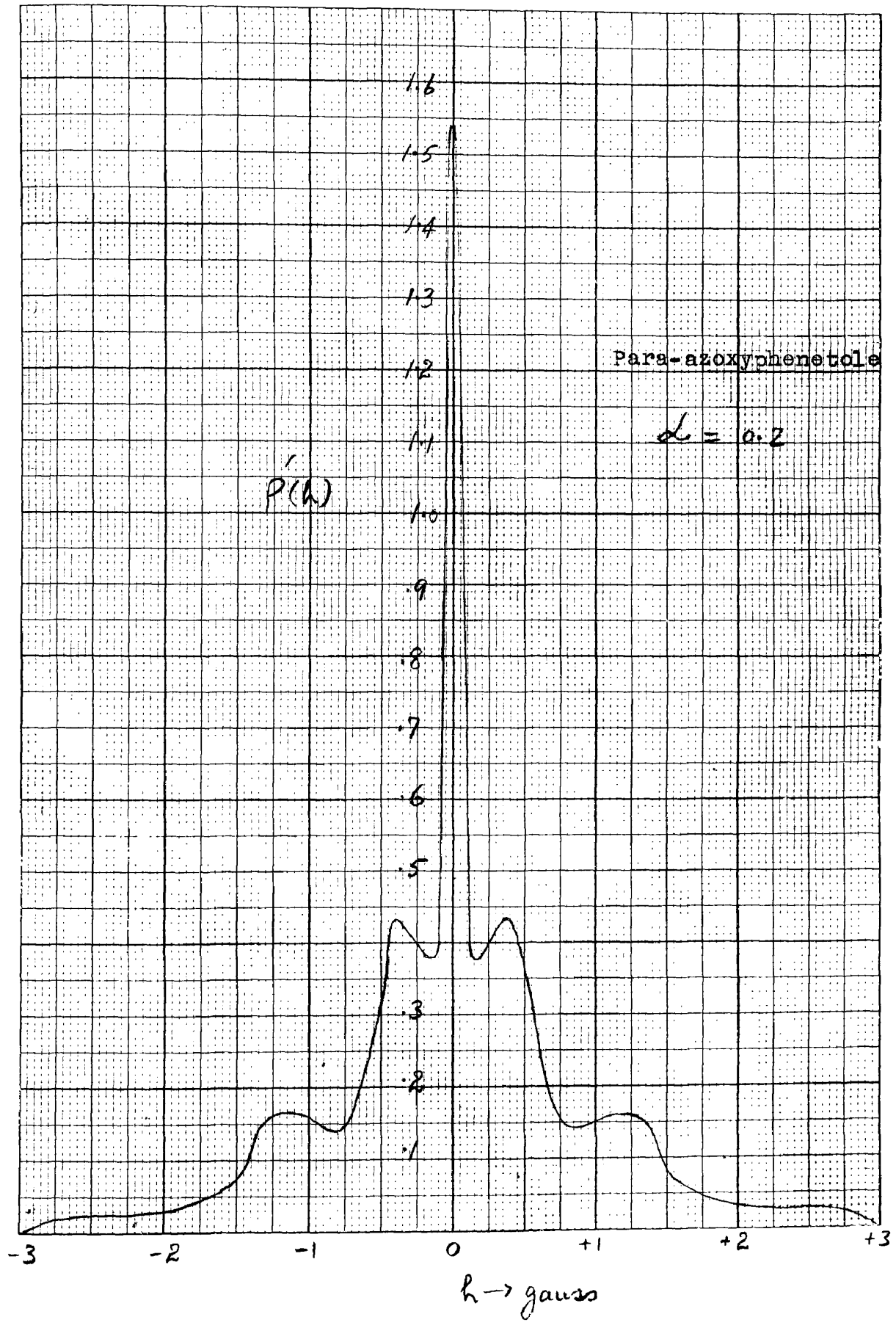
Para-azoxyphenetole
α = 0.2
P'(h)
1.6
1.5
1.4
1.3
1.2
1.1
1.0
.9
.8
.7
.6
.5
.3
.2
.1
-3
-2
-1
0
+1
+2
+3
h → gauss

Figure 25

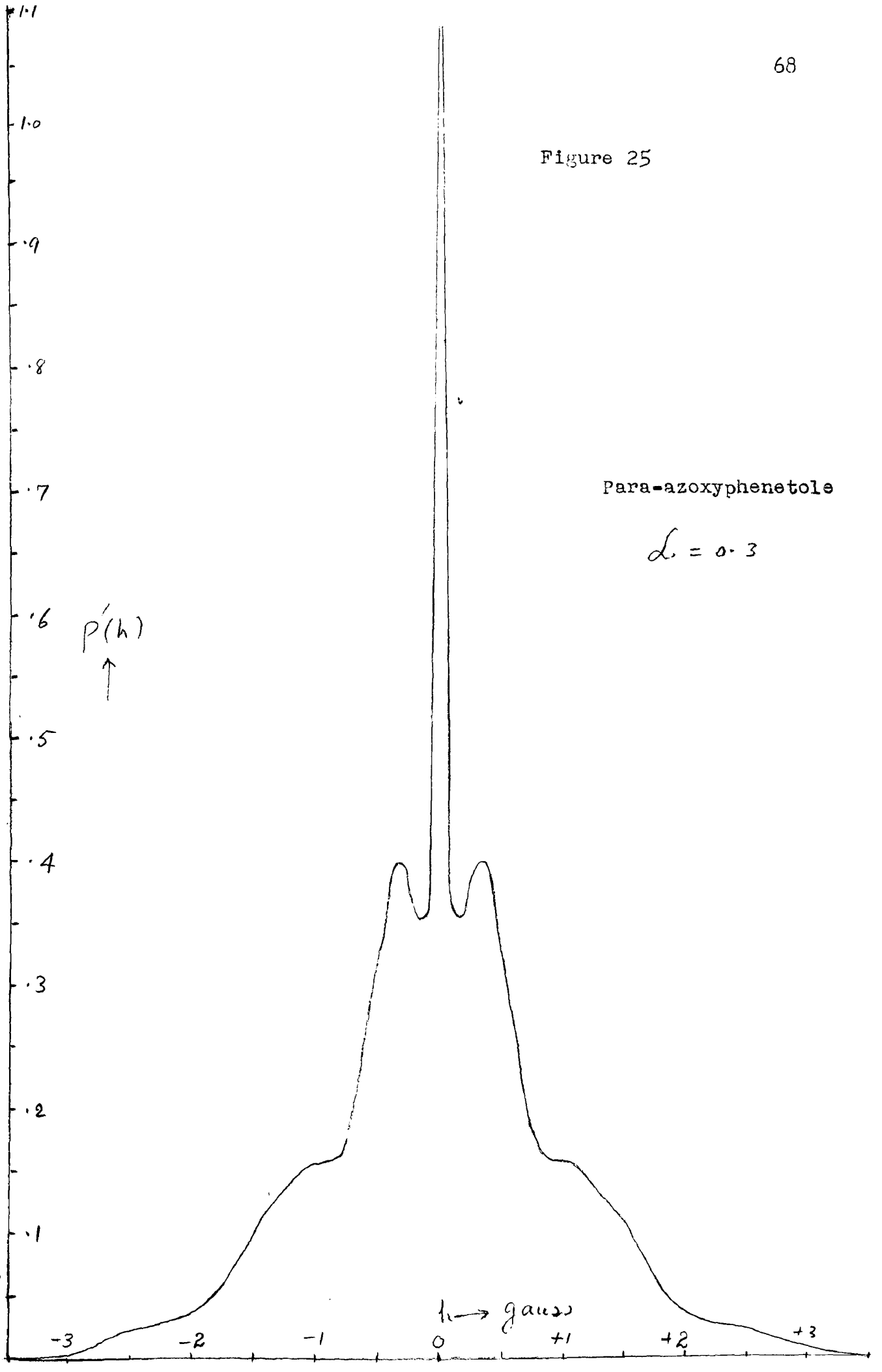

Para-azoxyphenetole

$\alpha = 0.3$

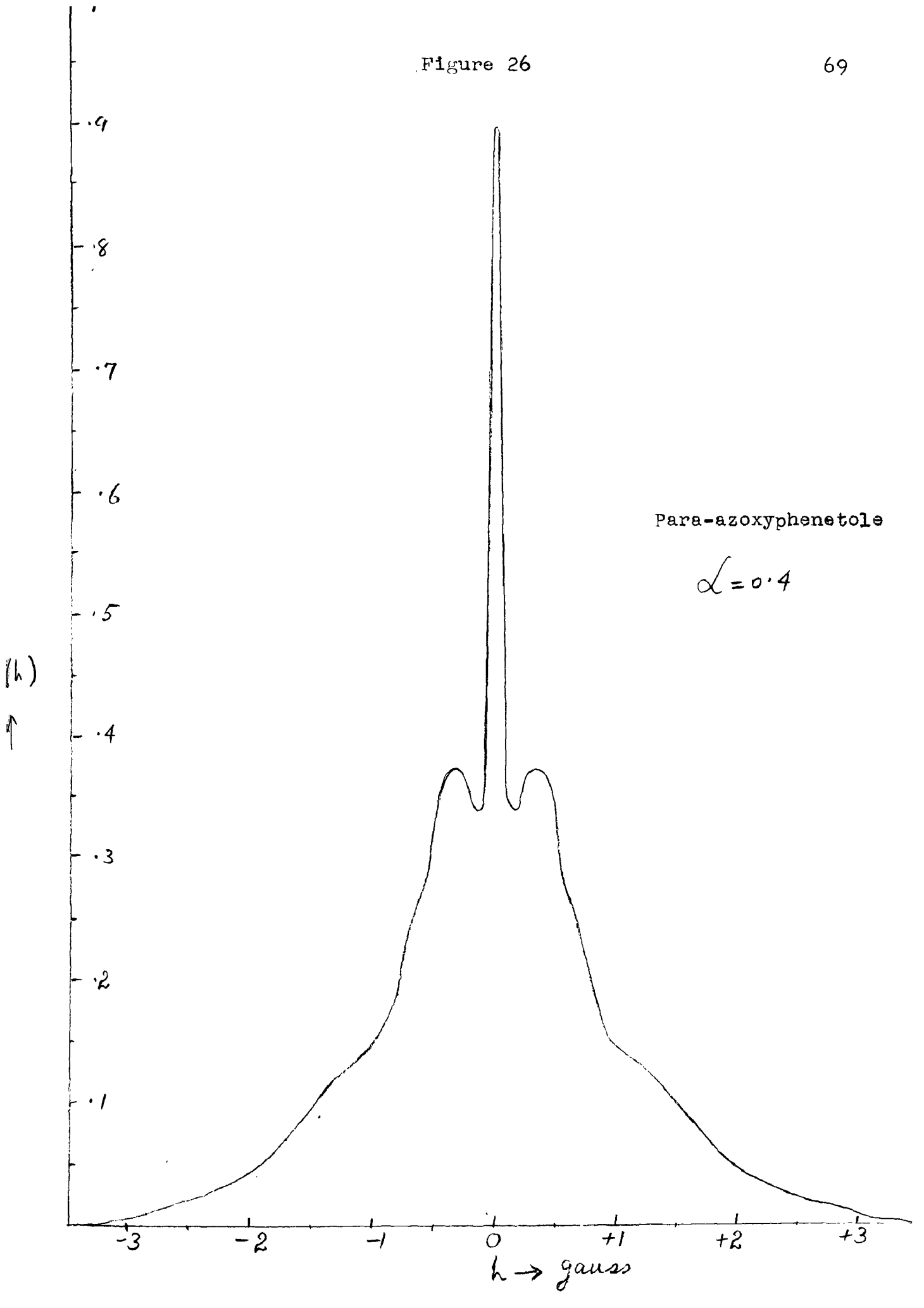
·9
·8
·7
·6
·5
·4
·3
·2
·1
I(h)
-3
-2
-1
0
+1
+2
+3
h → gauss
Para-azoxyphenetole
α = 0·4

$\sigma_1 = 0.204$ gauss

$\sigma_2 = 0.170$ gauss

(3) For $\alpha = 0.3$

$\sigma_1 = 0.306$ gauss

$\sigma_2 = 0.255$ gauss

If we look carefully on the line shape plots of para-azoxyanisole, shown in Figures 21, 22 and 23 for α values of 0.1, 0.2 and 0.3 respectively, one notices that the separation of the outer peaks is hardly affected by the external broadening in the above range. In Figure 21 the central line is too high and there are dips in the outer peaks. Both of these objections are reduced as the broadening is increased as shown in Figures 22 and 23. A comparison of the line shapes of Figures 22 and 23 of para-azoxyanisole with that of its experimental line shape in Figure 9 shows that it and the theoretical curve for $\alpha = 0.2$ and 0.3 are almost identical except for the facts that the central line of the theoretical curves is too high and the outer "humps" do not appear in the experimental lines. As the signal to noise ratio was not too good, it is possible that we might have failed to observe the outer "humps" in the line. Recently it has been noticed from one of Dr. Gutowsky's differential plots on para-azoxyanisole that when it is integrated it gives some indication of outer "humps" in the line.

For the case of para-azoxyphenetole the values of α

used are 0.2, 0.3 and 0.4 and are shown in Figures 24, 25 and 26 respectively with the following values of σ_i for the different groups of the molecule:

Para-azoxyphenetole

(1) $\alpha_i = 0.2$

$\sigma_1 = 0.204$ gauss

$\sigma_2 = 0.0848$ gauss

$\sigma_3 = 0.0550$ gauss

(2) $\alpha_i = 0.3$

$\sigma_1 = 0.306$ gauss (58b)

$\sigma_2 = 0.1272$ gauss

$\sigma_3 = 0.0825$ gauss

(3) $\alpha_i = 0.4$

$\sigma_1 = 0.408$ gauss

$\sigma_2 = 0.1696$ gauss

$\sigma_3 = 0.1100$ gauss

For $\alpha = 0.2$, the central line is quite high and the outer peaks are also quite sharp. But as we increase the value of α, the central line decreases in its height. Also, the sharpness of the outer peaks decreases with the increase in the value of α until at $\alpha = 0.4$ the outer peaks have practically been removed by the broadening effect and are no longer resolved.

It may be noted that the inner peaks are due in large measure to the central component of the primitive line shape as shown in Figure 19. The distance between the outer peaks

as well as in the inner peaks is hardly affected by the external broadening in this range.

A comparison of the line shape of Figure 24 for $\alpha = 0.2$ with the experimental line shape for para-azoxyphenetole at temperature 144° C in Figure 13e shows that it and the theoretical curve are almost identical in shape except that the central line is too high and the outer peaks are not as wide as shown experimentally. The explanation of the fact that the outer "humps" of the theoretical line were not observed experimentally is possibly the same as given in para-azoxyanisole. Similarly, line shapes in Figures 25 and 26 compare quite favorably with those of Figures 13b and 13a at temperatures 159° C and 166° C, respectively. At low temperature the outer peaks are farther apart experimentally than shown theoretically. The possible explanation for this is that there is an addition of another group, i.e., CH_2 group in the molecule of para-azoxyphenetole which was not present in the case of para-azoxyanisole and so the probability of interaction between the different groups of the molecule has increased, especially at low temperature and consequently broadens the lines. But in general the agreement between the theoretical and experimental curves shows that the theory based on a random orientation of swarms gives results which are at least in qualitative agreement with the experiment. The agreement is certainly much better than that obtained by use of the hypothesis of

complete orientation. In order to complete this discussion of random orientation of the molecular axes with the magnetic field, we calculate the various moments of the theoretical line shape and compare the results for the second moment with that of its experimental value.

The nth moment of the unbroadened distribution function P(h) is given by

$$\overline{h^n} = \sum_{i=1}^{i=N} \int_{-2\lambda_i}^{2\lambda_i} h^n p_i(h)\, dh , \tag{59}$$

where $p_i(h)$ is given by Eq. (47).

Therefore

$$\overline{h^n} = \sum_{i=1}^{i=N} \frac{\sqrt{3}\ \omega_i}{6\ \lambda_i} \left\{ \int_{-2\lambda_i}^{\lambda_i} h^n \left(1-\frac{h}{\lambda_i}\right)^{-1/2} dh + \int_{-\lambda_i}^{2\lambda_i} h^n \left(1+\frac{h}{\lambda_i}\right)^{-1/2} dh \right\}$$

$$= \sum_{i=1}^{i=N} \omega_i \lambda_i \frac{1}{\sqrt{3}} \int_0^3 \frac{(\xi-1)^n}{\sqrt{\xi}}\, d\xi \tag{60}$$

$$= \sum_{i=1}^{i=N} \omega_i \lambda_i^n\ b_n$$

where $$b_n = \frac{1}{\sqrt{3}} \int_0^3 \frac{(\xi-1)^n}{\sqrt{\xi}}\, d\xi \tag{60a}$$

$$(\xi-1)^n = \xi^n - n\xi^{n-1} + \frac{n(n-1)}{2!}\xi^{n-2} - \frac{n(n-1)(n-2)}{3!}\xi^{n-3}$$

$$\therefore \int_0^3 \frac{(\xi-1)^n}{\sqrt{\xi}}\, d\xi = \int_0^3 \sum_{k=0}^{k=n} \frac{(-1)^k\, n!}{(n-k)!} \cdot \frac{\xi^{n-k-1/2}}{k!}\, d\xi$$

$$= \sqrt{3} \sum_{k=0}^{k=n} \frac{2(-1)^k}{2(n-k)+1} \frac{n!}{(n-k)!} \frac{(3)^{n-k}}{k!}$$

$$\therefore \overline{h^n} = \sum_{i=1}^{i=N} \omega_i \lambda_i^n \sum_{k=0}^{k=n} \frac{2(-1)^k \; n! \; (3)^{n-k}}{2(n-k)+1 \; (n-k)! \; k!}$$

$$= b_n \sum_{i=1}^{i=N} \omega_i \lambda_i^n \tag{61}$$

$$\text{where} \quad b_n = \sum_{k=0}^{k} \frac{2(-1)^k}{2(n-k)+1} \frac{n!}{(n-k)!} \frac{(3)^{n-k}}{k!} \tag{62}$$

$$b_2 = 1.6 \tag{63}$$

$$b_4 = 2.74286 \tag{64}$$

$$b_6 = 6.7772 \tag{65}$$

$$b_8 = 20.008226$$

Calculated values of the moments

$\overline{h^n} = b_n \sum_{i=1}^{i=N} \omega_i \lambda_i^n$ is given below.

For the case of para-azoxyanisole

$$\overline{h^2} = 1.1965 \text{ gauss}^2$$

$$\overline{h^4} = 3.989 \text{ gauss}^4 \tag{66}$$

$$\overline{h^6} = 19.41 \text{ gauss}^6$$

$$\overline{h^8} = 115.1 \text{ gauss}^8$$

For the case of para-azoxyphenetole

$$\begin{aligned} \overline{h^2} &= 0.82016 \text{ gauss}^2 \\ \overline{h^4} &= 2.63 \text{ gauss}^4 \\ \overline{h^6} &= 13.35 \text{ gauss}^6 \\ \overline{h^8} &= 86.0384 \text{ gauss}^8 \end{aligned} \tag{67}$$

The expression for the moments given in Eq. (62) is quite general for the cases in which Eq. (41a) (~~40~~) is valid. One could obtain higher moments from the simple expression very easily. Van Vleck has calculated moments only up to fourth order. If that technique is continued further for higher moments, it becomes too difficult to get a simplified expression for higher moments. In obtaining the above moments, we have made use of the distribution function P(h) given in Eq. (47). One could also find the second moment without knowing the distribution function P(h) by making use of Eq. (30). This device [31] has been used for the calculation of the second moment for the case of para-azoxyanisole, and could also be used for the case of para-azoxyphenetole.

In order to calculate the experimental value of second moments of these compounds, the area of the curve obtained from $h^2P(h)$, where P(h) represents any of the experimental line shape, was normalized by its original area, and thus gives the required second moment of that particular curve. The areas of all these enlarged curves were measured with the

---

31. Spence, Gutowsky and Holm, op. cit., p. 1891.

help of a planimeter. For the case of para-azoxyanisole, the experimental values of second moments are 0.95 gauss^2, 1.15 gauss^2 and 1.25 gauss^2 at 134° C, 127° C, and 118° C, respectively. In the case of para-azoxyphenetole, the experimental values of second moments varies from 1.75 gauss^2 at temperature 166° C to 5 gauss^2 at temperature 140° C. If we compare the above values of para-azoxyanisole with those derived in Eq. (66) for the second moment, we notice that the calculated value lies in the range of our observation. But if we compare the line shapes from which these moments have been calculated, we have to consider the broadening effect which has not been taken into consideration in the calculation of Eq. (66). For the case of para-azoxyphenetole the calculated value of second moments in Eq. (67) is much less than the experimental values. So the next step would be to calculate the effect of a Gaussian broadening function on the moments. The distribution function under the effect of Gaussian broadening is given by:

$$P'(h) = \sum_{i=1}^{i=N} p_i'(h) \tag{69}$$

where $$p_i'(h_1) = \int_{-\infty}^{\infty} g_i(h-h_1)\, p_i(h_1)\, dh_1$$

where $$g_i(h-h_1) = \frac{1}{2\pi\sigma_i}\, e^{-\frac{(h-h_1)^2}{2\sigma_i^2}} \tag{70}$$

The moments of the Gaussian broadening distribution are

$$\overline{h^n}' = \sum_{i=1}^{i=N} \int_{-2\lambda_i}^{2\lambda_i} h^n p_i'(h)\, dh$$

$$= \sum_{i=1}^{i=N} \int_{-2\lambda_i}^{2\lambda_i} h^n \left[\int_{-\infty}^{+\infty} g_i(h-h_1)\, p_i(h_1)\, dh_1 \right] dh \qquad (71)$$

$$= \sum_{i=1}^{i=N} \int_{-2\lambda_i}^{2\lambda_i} h^n \left[\int_{-\infty}^{+\infty} \frac{1}{\sqrt{2\pi}\,\sigma_i} e^{-\frac{(h-h_1)^2}{2\sigma_i^2}} p_i(h_1)\, dh_1 \right] dh$$

$$= \sum_{i=1}^{i=N} \int_{-2\lambda_i-h_1}^{2\lambda_i-h_1} (\xi+h_1)^n \left[\int_{-\infty}^{+\infty} \frac{e^{-\frac{\xi^2}{2\sigma_i^2}}}{\sqrt{2\pi}\,\sigma_i} p_i(h_1)\, dh_1 \right] d\xi$$

where $h-h_1=\xi$; $dh=d\xi$ (72)

For simplicity we first take the case for n = 2

$$\overline{h^2}' = \sum_{i=1}^{i=N} \int_{-2\lambda_i-h_1}^{2\lambda_i-h_1} \int_{-\infty}^{\infty} (\xi+h_1)^2 \frac{e^{-\frac{\xi^2}{2\sigma_i^2}}}{\sqrt{2\pi}\,\sigma_i} p_i(h_1)\, dh_1\, d\xi \qquad (73)$$

$$= \sum_{i=1}^{i=N} \int_{-2\lambda_i-h_1}^{2\lambda_i-h_1} \int_{-\infty}^{+\infty} (\xi^2 + h_1^2 + 2\xi h_1) \frac{e^{-\frac{\xi^2}{2\sigma_i^2}}}{\sqrt{2\pi}\,\sigma_i} p_i(h_1)\, dh_1\, d\xi$$

$$= \sum_{i=1}^{i=N} \left(\overline{h^2} + \omega_i \sigma_i^2 \right)$$

where $\overline{h^2}$ is the unbroadened second moment

$$= \sum_{i=1}^{i=N} \omega_i \left(h_2 \lambda_i^2 + \sigma_i^2 \right) \qquad (74)$$

Similarly, the higher moments may be calculated by making use of Eq. (62) for the unbroadened part, together with the Gaussian broadening part, for which the general expression

for the nth moment is given by[32]

$$\overline{\xi^n} = \int_{-\infty}^{\infty} \frac{\xi^n}{\sqrt{2\pi}\,\sigma} e^{-\frac{\xi^2}{2\sigma^2}} d\xi = [1\cdot 3\cdot 5\cdot \cdots\cdots (n-1)]\sigma^n \quad (75)$$

if n is even

$= 0$ if n is odd

$$\overline{h^4}' = \sum_i \omega_i (b_4 \lambda_i^4 + 6 b_2 \lambda_i^2 \sigma_i^2 + 3\sigma_i^4)$$

$$\overline{h^6}' = \sum_i \omega_i (b_6 \lambda_i^6 + 15 b_4 \lambda_i^4 \sigma_i^2 + 45 b_2 \lambda_i^2 \sigma_i^4 + 15\sigma_i^6) \quad (76)$$

$$\overline{h^8}' = \sum_i \omega_i (b_8 \lambda_i^8 + 28 b_6 \lambda_i^6 \sigma_i^2 + 210 b_4 \lambda_i^4 \sigma_i^4 + 420 b_2 \lambda_i^2 \sigma_i^6 + 105\sigma_i^8)$$

etc.- - - - - -

Now we shall calculate the second moment under the broadening effect by amking use of expression in Eqs. (58a), (58b) and (75).

For the case of para-azoxyanisole the calculated second moments are

$$\overline{h^2}' = 1.2115 \text{ gauss}^2 \text{ for } \alpha = 0.2$$
$$\overline{h^2}' = 1.23035 \text{ gauss}^2 \text{ for } \alpha = 0.3 \quad (77)$$

These values are quite close to the values observed near 125° C and 121° C and also the calculated line shapes coincide fairly well with the experimental line shapes

---

32. Margenau and Murphy, D. Van Nostrand Company, (1943), p. 422.

except that the central line is too high.

For the case of para-azoxyphenetole, the calculated second moment under the broadening effect is given by

$$\overline{h^2}' = 0.93041 \text{ gauss}^2 \text{ for } \alpha = 0.2$$
$$\overline{h^2}' = 0.86126 \text{ gauss}^2 \text{ for } \alpha = 0.4 \qquad (78)$$

Although the above values of the calculated second moments do not lie in the range of observed values, the line shapes in general agree fairly well with the experimental line shapes excepting that as in para-azoxyanisole, the central line is too high.

Thus we see that excepting the calculated high value of the central line in para-azoxyanisole and para-azoxyphenetole and the low value of second moment in para-azoxyphenetole, the theory based on a random orientation of swarm gives quite satisfactory results. No doubt the second moment and the other higher moments are very sensitive to the exact line shape in the outer protons of the line, and as the outer portions of our observed line shapes are not known exactly on account of low signal to noise ratio, we can expect a small variation in the experimental and the calculated value of the second moment of the line shape of para-azoxyanisole and para-azoxyphenetole. The above explanation may be satisfactory in the case of para-azoxyanisole, but certainly is not satisfactory in the case of para-azoxyphenetole, as in the latter case the difference in the calculated and the experimental value of the second moment is too large to be

explained on the basis of inaccuracies in the outer portion of the line.

In order to explain the experimental results of the high value of the second moment in the case of para-azoxyphenetole and of small values of the central lines in para-azoxyanisole and para-azoxyphenetole, we must consider the case of partial orientation of the molecular axes with the magnetic field.

In order to discuss the case of partial orientation, we modify the Eq. (44) as follows:

$$dN = \frac{N}{2} g(\beta_0) \sin\beta_0 \, d\beta_0 \qquad (79)$$

An approximate form of the function $g(\beta_0)$ for liquid crystals has been suggested by Onsager[33]. He gives

$$g(\beta_0) = K \frac{\cosh(K\cos\beta_0)}{\sinh K} \qquad (80)$$

Eq. (79) becomes

$$dN = \frac{N}{2}\left(K \frac{\cosh(K\cos\beta_0)}{\sinh K}\right)\sin\beta_0 \, d\beta_0 \qquad (81)$$

where the parameter K presumably depends upon temperature.

K = 0 corresponds to random orientation

K = ∞ corresponds to complete orientation.

The distribution for the ith group is then given by Eq. (82) instead of Eq. (47).

$$p_i(h,K) = \frac{\sqrt{3}}{6\lambda_i}\omega_i \left(K \frac{\cosh\left(\frac{K}{\sqrt{3}}\left(1-\frac{h}{\lambda_i}\right)^{1/2}\right)}{\sinh K}\right)\left(1-\frac{h}{\lambda_i}\right)^{-1/2}$$

$$-2\lambda_i \leq h \leq -\lambda_i$$

---

33. Onsager, Ann. N. Y. Acad. Sci., 51(4):627

$$\rho_i(h,K) = \frac{\sqrt{3}}{6\lambda_i}\omega_i\left\{K\frac{\cosh\left(\frac{K}{\sqrt{3}}\left(1-\frac{h}{\lambda_i}\right)^{1/2}\right)}{\sinh K}\left(1-\frac{h}{\lambda_i}\right)^{-1/2} + K\frac{\cosh\left(\frac{K}{\sqrt{3}}\left(1+\frac{h}{\lambda_i}\right)^{1/2}\right)}{\sinh K}\left(1+\frac{h}{\lambda_i}\right)^{-1/2}\right\}$$

$$\rho_i(h,K) = \frac{\sqrt{3}}{6\lambda_i}\omega_i\left\{K\frac{\cosh\left(\frac{K}{\sqrt{3}}\left(1+\frac{h}{\lambda_i}\right)^{1/2}\right)}{\sinh K}\left(1+\frac{h}{\lambda_i}\right)^{-\frac{1}{2}}\right\} \qquad -\lambda_i \le h \le \lambda_i \tag{82}$$

$$\rho_N(h,K) = \omega_N\,\delta(0,h) \qquad \lambda_i \le h \le 2\lambda_i$$

We can now calculate the broadened distribution function by inserting the above expressions for $\rho_i(h)$ in Eq. (49a). Similarly, the broadened moment for the case of partial orientation can be calculated from Eqs. (74) and (76), excepting that b_n in Eq. (60a) is replaced with the quantity,

$$b_n(K) = \frac{1}{\sqrt{3}}\int_0^3 \frac{(\xi-1)^n}{\sqrt{\xi+1}}\left(K\frac{\cosh\left(\frac{K}{\sqrt{3}}\sqrt{\xi}\right)}{\sinh K}\right)d\xi \tag{83}$$

$$= \frac{K}{\sinh K}\int_{-1}^{} (3\rho^2-1)^n \cosh K\rho\, d\rho$$

We note in particular that

$$b_n(0) = b_n$$

and

$$b_2(K) = \frac{K}{\sinh K}\int_{-1}^{+1}(3\rho^2-1)^2\cosh K\rho\, d\rho$$

$$= 8\left[1+\frac{24}{K^2}+\frac{54}{K^4}-6\frac{\coth K}{K}\left(1+\frac{9}{K^2}\right)\right] \tag{84}$$

The height of the line at the center (h = 0) for partial orientation is given by

$$P'(0,K) = \frac{W_N}{\sqrt{2\pi}} \frac{1}{\sigma_{N-1}} + \sum_{i=1}^{i=N-1} \frac{2}{\sqrt{6}} \frac{w_i}{\lambda_i} G(1,\alpha_i)\, K \frac{\cosh K\left(\frac{K}{\sqrt{3}}\right)}{\sinh K}$$

$$\simeq \frac{W_N}{\sqrt{2\pi}} \frac{1}{\sigma_{N-1}} + \sum_{i=1}^{i=N-1} \frac{1}{\sqrt{3}} \frac{w_i}{\lambda_i} K \frac{\cosh K\left(\frac{K}{\sqrt{3}}\right)}{\sinh K} \qquad (85)$$

where function $G(1,\alpha_i)$ is given in Figure 20 and is approximately equal to $\frac{1}{\sqrt{2}}$ for all small α_i . The corresponding expression of P'(0) for random orientation is given by

$$P'(0,0) \simeq \frac{W_N}{\sqrt{2\pi}} \frac{1}{\sigma_{N-1}} + \sum_{i=1}^{i=N-1} \frac{1}{\sqrt{3}} \frac{w_i}{\lambda_i} \qquad (86)$$

In the above discussion the factor

$$F(K) = K \frac{\cosh\left(K/\sqrt{3}\right)}{\sinh K}$$

has the form shown in Figure 27.

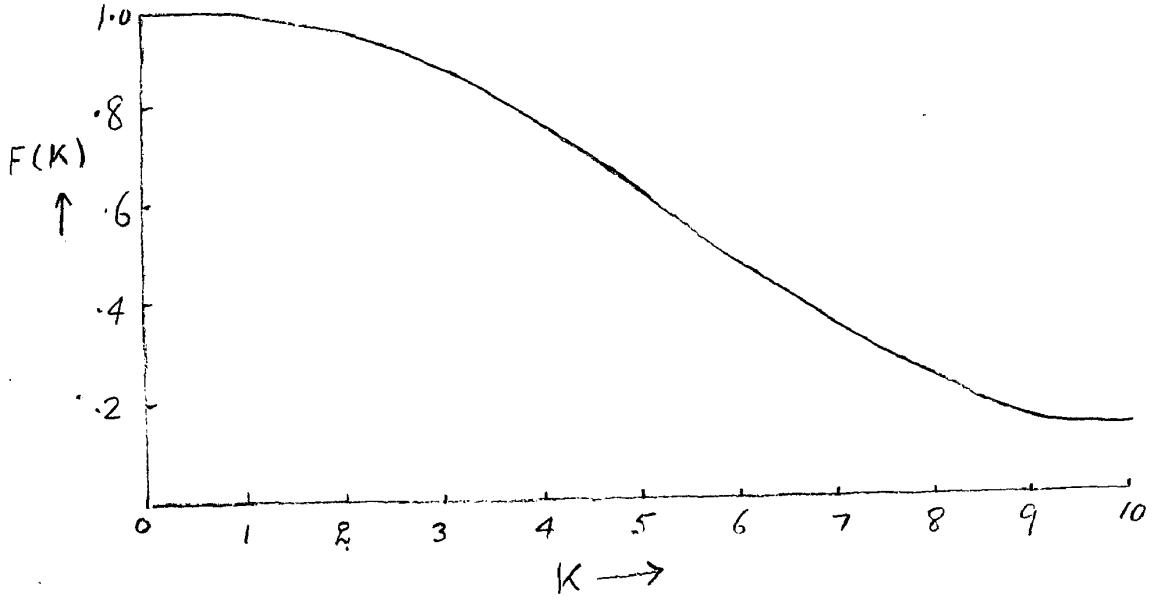

Figure 27

Thus since $F(K) < 1$ for $K > 0$ partial orientation will reduce the height of the center of the line in each case.

In order to calculate the values of K as a function of temperature we first note the expression given by Zwetkoff[34] for $\overline{\sin^2\beta_0}$

$$\overline{\sin^2\beta_0} = \frac{1}{2}\int_0^{\pi} g(\beta_0)\sin^3\beta_0\, d\beta_0 \qquad (87)$$

Here $g(\beta_0)$ is given by Eq. (80)

$$\therefore \overline{\sin^2\beta_0} = 2\left[\frac{1}{K}\coth K - \frac{1}{K^2}\right]$$

and

$$\overline{\cos^2\beta_0} = 1 + 2\left[\frac{1}{K^2} - \frac{\coth K}{K}\right] \qquad (88)$$

$$= \frac{1}{3} + \frac{2K^2}{45} - \frac{4}{945}K^3 + \frac{2}{4725}K^5 - \cdots \qquad (89)$$

Figure 28 shows the relation between $\overline{\cos^2\beta_0}$ and K. Zwetkoff has given experimental values of long range order parameter S, as a function of temperature $^{\circ}$ C for para-azoxyanisole where

$$S = \frac{1}{2}\overline{\left(3\cos^2\beta_0 - 1\right)} \qquad (90)$$

His results are given in the first three columns of the following table (Table I).

Figure 29 shows the relation between $\overline{\cos^2\beta_0}$ and temperature $^{\circ}$ C for para-azoxyanisole. Now from the plots

34. Zwetkoff, Acta Physichimica (USSR) 16:132 (1942).

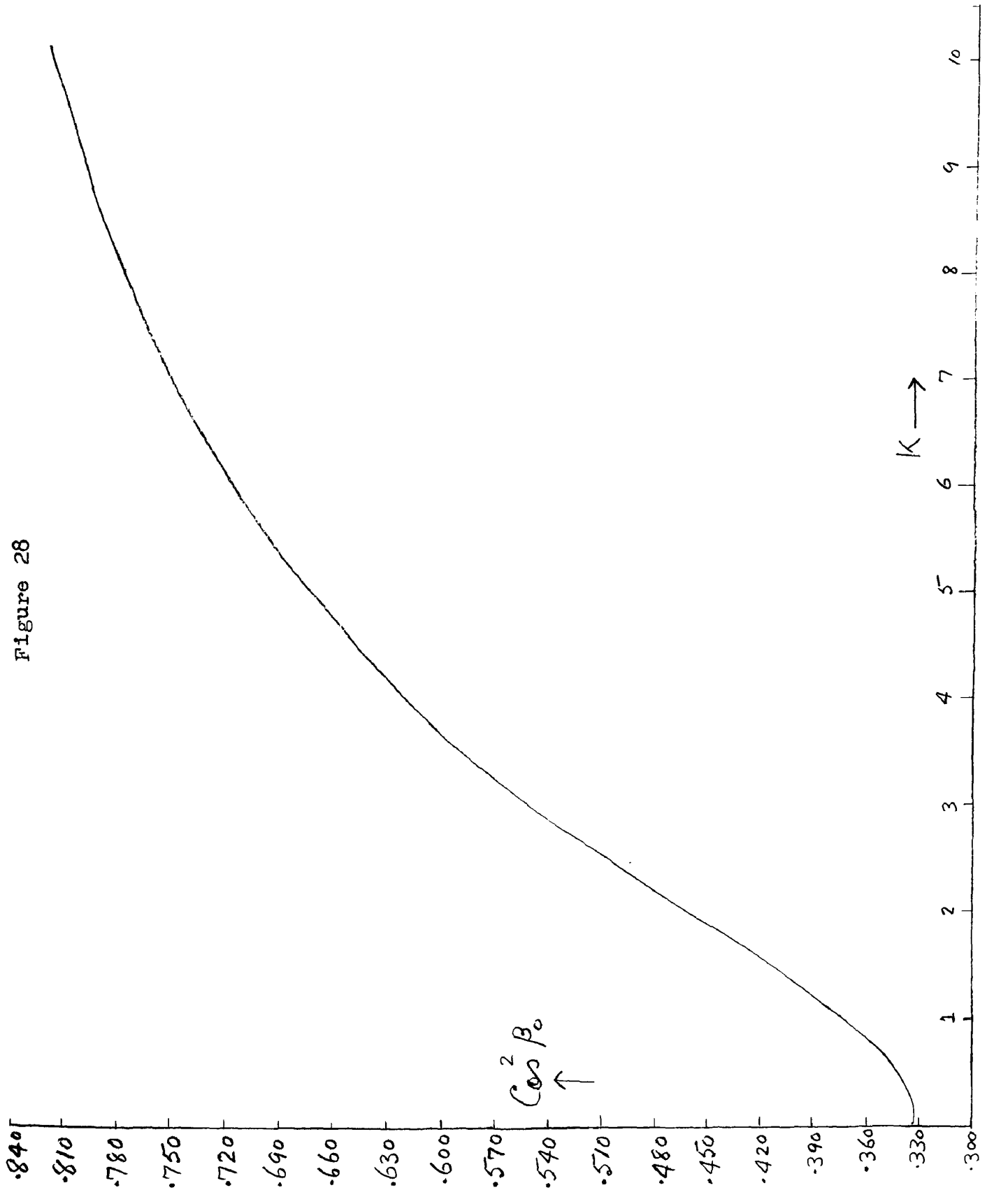
.840
.810
.780
.750
.720
.690
.660
.630
.600
.570
.540
.510
.480
.450
.420
.390
.360
.330
.300
$\cos^2 \beta_o$
1
2
3
4
5
6
7
8
9
10
K ⟶

Figure 28

TABLE I

Temperature (° C)	S	$\overline{\omega_2^2 \beta_0}$	K	$\int_{G_2}(K)$
117.0	.68	.787	8.25	4.3272
121.0	.65	.767	7.5	4.1272
122.0	.64	.760	7.2	4.0256
128.0	.58	.720	6.0	3.6696
128.5	.57	.713	5.85	3.6200
130.0	.54	.693	5.35	3.4424
132.0	.50	.667	4.8	3.2424
135.0	.40	.600	3.6	2.7680

of Figures 28 and 29 we construct another plot relating K and temperature ° C, which is shown in Figure 30 and for which data is tabulated in the first and the fourth columns of Table I. From the data given in Table I we may now compute the second moment at different temperatures by assuming different values of α_i. Furthermore it is also possible to evaluate the quantity $P'(0,0)/P'(0,K)$ which is a measure of the relative reduction of the amplitude of the central line produced by partial orientation. The results are given in Table II.

The comparison between the calculated and experimental second moments is very unsatisfactory, since the calculated values of $\overline{h}^2$ are the order of twice the experimental values.

Figure 29

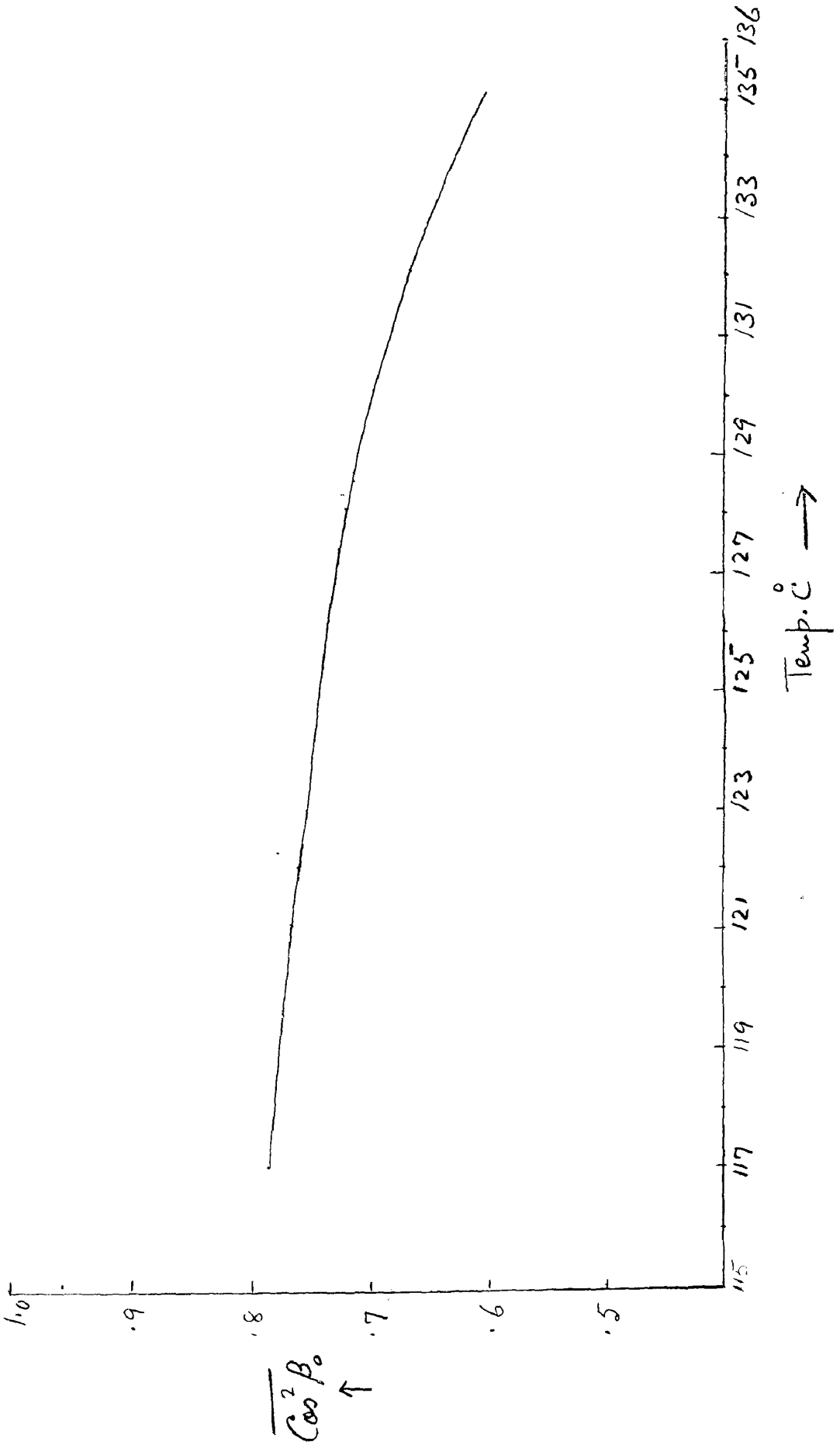
1.0
.9
.8
.7
.6
.5
$\overline{\cos^2\beta_0}$ ↑
115
117
119
121
123
125
127
129
131
133
135
136
Temp. C° →

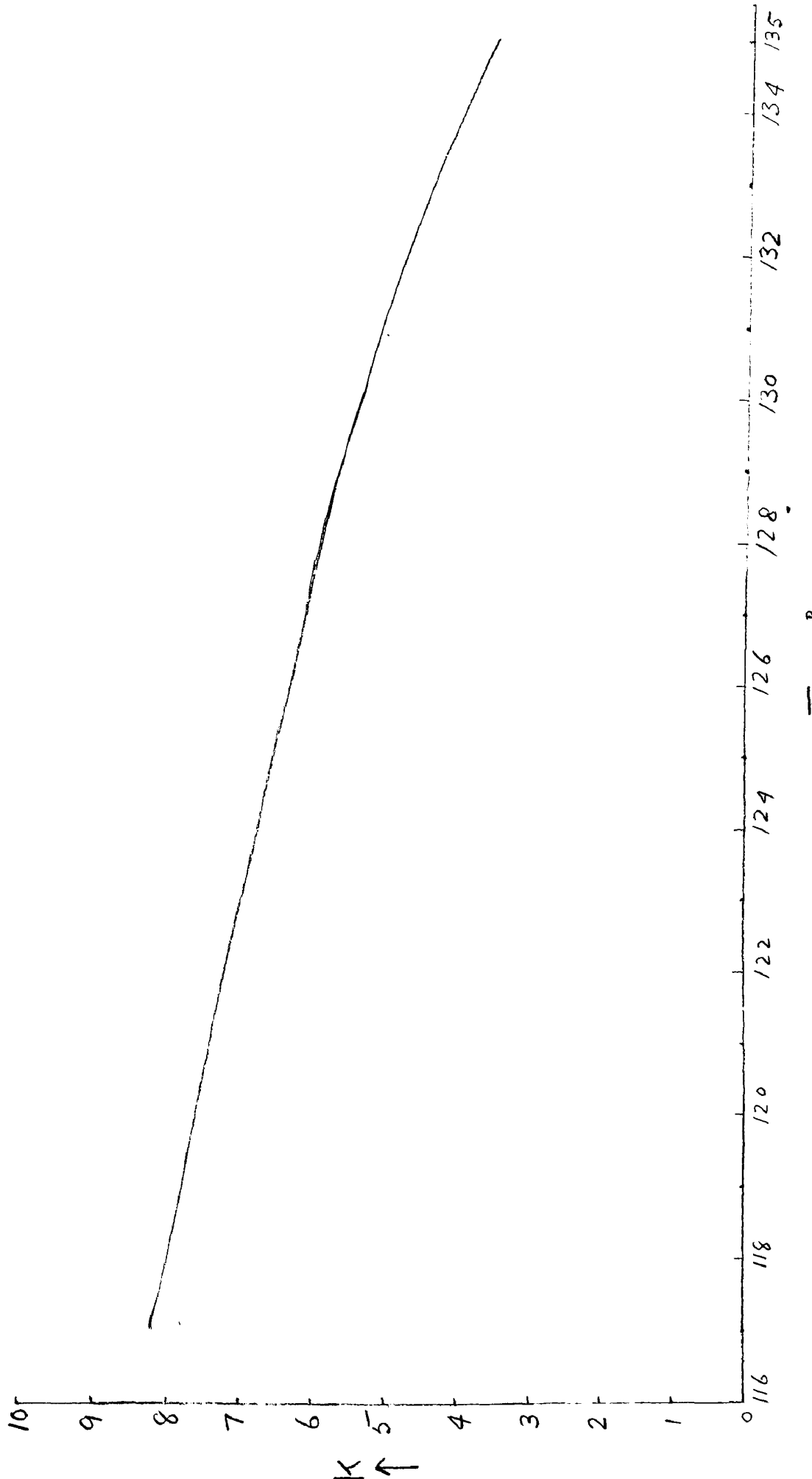
K
10
9
8
7
6
5
4
3
2
1
0
116
118
120
122
124
126
128
130
132
134
135
Temp C°

Figure 30

TABLE II

CALCULATED VALUES OF $\overline{h^2}$

Temperature (° C)	$\overline{h^2}$ (= 0.1)	$\overline{h^2}$ (= 0.2)	$\overline{h^2}$ (= 0.3)	$\overline{h^2}$ (exptl.)	$\frac{\rho'(0,0)}{\rho'(0,k)}$
117	3.23	3.24	3.26	1.25	.752
125	3.08	3.09	3.11	1.15	.796
134	2.18	2.20	2.22	0.95	.920

The reduction of the amplitude of the central line is encouraging, but in itself is not sufficient to justify the assumption of partial orientation. We are therefore faced with three alternatives. Either (1) Onsager's distribution function is much too crude to be used in this computation, (2) the orientation is essentially random, (3) the entire molecular model on which these computations are based are incorrect. If we disregard the third alternative temporarily we may cite one piece of evidence which appears to indicate that orientation does indeed exist in the liquid crystal phase of para-azoxyanisole and therefore the difficulty lies in the use of Onsager's distribution function. From Eq. (46a) we set

$$g(\beta_0)\, d(\cos\beta_0) = \frac{g(\beta_0)}{6\lambda_i \cos\beta_0}\, dh = D\left(\frac{h}{\lambda_i}\right)\frac{dh}{\lambda_i} \qquad (91)$$

Let β_{0m} be the value of β_0 at which the function D

is a maximum. The corresponding value of h is

$$\frac{h_m}{\lambda_i} = \pm \left(3\cos^2\beta_{0m} - 1\right) \tag{92a}$$

the satellite separation is then

$$\Delta h = 2\lambda_i\left(3\cos^2\beta_{0m} - 1\right) \tag{92b}$$

Zwetkoff's long range order parameter S is given by

$$2S = \overline{3\cos^2\beta_0 - 1} = -2\int_{0}^{\pi/2}\left(3\cos^2\beta_0 - 1\right)g(\beta_0)\,d(\cos\beta_0) \tag{93}$$

$$= 2\int_{-1}^{0}\frac{h}{\lambda_i}D\left(\frac{h}{\lambda_i}\right)\left(\frac{dh}{\lambda_i}\right)$$

We now make the assumption that D belongs to that class of distribution functions for which the mean and the mode of the function are approximately equal. Then from Eq. (93)

$$2S = \overline{3\cos^2\beta_0 - 1} \simeq 3\cos^2\beta_{0m} - 1 \tag{94}$$

For p-azoxyanisole the satellite lines should then occur at

$$h \simeq \pm 2\lambda_1 S = \pm(2.88)S \text{ gauss} \tag{95a}$$

$$h \simeq \pm 2\lambda_2 S = \pm(2.40)S \text{ gauss} \tag{95b}$$

If we assume that these lines coalesce to give a single pair of satellites at the average position

$$h \simeq \pm (2.64)S \text{ gauss} \tag{96}$$

the satellites' separation is

$$\Delta h \simeq (5.28)S \tag{97}$$

Table III compares the values of Δh calculated by this formula with the experimental values.

TABLE III

COMPARISON OF CALCULATED AND EXPERIMENTAL VALUES OF Δ h FOR PARA-AZOXYANISOLE

Temperature (° C)	Δh (exptl.)	Δh (calc.)
117.0	3.50	3.59
121.0	3.40	3.43
122.0	3.35	3.38
128.0	2.95	3.06
128.5	2.90	3.01
130.0	2.75	2.85
132.0	2.50	2.64
135.0	2.20	2.11

The agreement indicated here is well within the experimental error. Thus we have shown that there exists a class of distribution functions which give satellite separation in complete agreement with the experimental results for para-azoxyanisole.

Unfortunately there appears to be no data on the value

of S available for para-azoxyphenetole and therefore we cannot use Eq. (97) to calculate Δh. However, if we assume that a similar equation can also be applied to para-azoxyphenetole it might be used to predict the long order parameter S which has not thus far been reported in the literature.

TABLE IV

LONG RANGE ORDER PARAMETER S FOR PARA-AZOXYPHENETOLE COMPUTED FROM $\Delta h \approx 5.55\ S$

Temperature (° C)	Δh (exptl.)	S
138	5.55	1.00
144	5.50	0.99
147	5.40	0.97
150	5.33	0.96
154	5.1	0.92
155	5.0	0.90
158	4.7	0.85
160	4.4	0.79
163	3.9	0.70
166.6	3.0	0.54

We still cannot completely exclude the possibility that the molecular model we have employed is incorrect. In particular the intermolecular forces in liquid crystals are not well

understood and there does not as yet appear any positive evidence that one can exclude the possibility that the observed line shapes are produced by some complicated mixture of intramolecular and intermolecular effects. However, it seems that the points of agreement between the simple theory we have outlined here and the experimental results are too numerous to be a coincidence.

VI. SUMMARY

Nematic liquid crystals show an intermediate phase between the crystalline and normal liquid phase. They flow like ordinary liquids and show in the presence of an electric or magnetic field the anisotropy commonly associated with the crystalline state. X-ray studies show that in the liquid crystal phase there is an aggregation of molecules much larger in size than the aggregation of molecules in the liquid phase. It has been found that there is a discontinuity in the values of viscosity, static electric and magnetic susceptibility at the transition points of the liquid crystal states.

Phase transitions in nematic liquid crystals, such as para-azoxyanizole and para-azoxyphenetole from their liquid to their liquid crystal phase and from liquid crystal to their solid phase, have been observed by means of proton magnetic resonance. The magnetic resonance absorption was observed by means of a twin-T radio frequency bridge with conventionally associated components. The observations were made at a field of the order of 7300 gauss modulated at a frequency of 30 cps.

In the normal liquid state of both para-azoxyanisole and para-azoxyphenetole the line width is very narrow. At the transition point (135° C) between the liquid and the

liquid crystal phase of para-azoxyanisole the single line splits into three components and at the second transition point (118° C) the compound passes into the solid state and exhibits a wide line. In the case of para-azoxyphenetole the single line splits into three components at the transition point (166.6° C), between the liquid and the liquid crystal phase. At a very low temperature, in the liquid crystal range, five lines were observed. At the second transition point (138° C) the compound passes into the solid state and exhibits a wide line similar to that found in para-azoxyanisole.

The line shape that appears in the liquid crystal range of above compounds is found to be field independent and considered to be due to nuclear magnetic dipole interaction. The quantum mechanical results of the interaction between nuclear magnetic dipoles has been summarized in order to use them for explaining the experimental results. The theoretical analysis of the line shape found in the liquid crystal phase of these compounds has been attempted. This analysis is based on certain molecular models and certain assumptions about the orientation of the molecules under the influence of the external magnetic field. Theoretical line shape due to random orientation of the molecules with Gaussian external broadening has been used to interpret the experimental line shapes. Further coincidence between experimental and theoretical values is

brought through the hypothesis of partial orientation of the molecules.

In order to obtain a further check on the proposed explanation of the structure arising in the liquid crystal range, it would be profitable to replace the hydrogen on the end groups of para-azoxyanisole by deutrons and to observe the signal in the liquid crystal range. According to the above proposed interaction, only the lines arising from the hydrogens on the benzene ring should appear with no further resonance line appearing from the deutrated group of the molecule.

VII. REFERENCES

Alpert, N. L. Phys. Rev. 75:398 (1949).

Anderson, H. L. Phys. Rev. 76:1462 (1949).

Andrew and Bersohn. J. Chem. Phys. 18:159 (1950).

Bloembergen, N. "Nuclear magnetic relaxation" (Martinus Nijhoff) (1948).

Carr, E. and Spence, R. Bull. Am. Physc. Soc. 28(1):8 (1953).

Chatelain, Par Pierre. Acta Crysta I:315 (1948).

Faraday Society. "Discussion on liquid crystals" 2 (1933).

Foex and Royer. Compt. rend. 180:1912 (1925).

Foex. J. de Phys. et le Rad. VI(X):421 (1929).

Frankel, J. Kinetic theory of liquids. London: Oxford University Press (1946).

Goldstein, Herbert. Classical mechanics. Addison-Wesley Press (1951).

Gordy. Microwave spectroscopy. John Wiley & Sons (1953).

Gutowsky and Pake. J. Chem. Phys. 18:162 (1950).

Jacobson, Wangsness. Phys. Rev. 73:942 (1948).

Kast, W. Ann. Physik 83:418 (1927).

Kreutzer. Ann. Physik 33:192 (1938).

Krishanan, K. S. Proc. Ind. Soc. Cong. Madras Session (1929).

Landau, L. Physik Zeits. Sowjetunion 11(26):545 (1937).

London, F. J. Phys. Radium 8:397 (1937).

Mair, W. Z. Naturforschung 8:458 (1927).

Mangun, M. G. Compt. rend. 152:1680 (1911).

Margenau and Murphy. D. Van Nostrand Company (1943).

Onsager. Ann. N. Y. Acad. Sci. 51(4):627

Pake, G. E. J. Chem. Phys. 16:327 (1948).

Pauling, L. J. Chem. Phys. 4:673 (1936).

Pauling. Nature of the chemical bond. Cornell University Press (1948).

Powell and Gutowsky. J. Chem. Phys. 21:1704 (1953).

Peirce, B. O. A short table of integrals. Ginn & Co. (1910).

Schiff, Leonard I. Quantum mechanics. McGraw-Hill Book Company (1949).

Spence, Gutowsky and Holm. J. Chem. Phys. 21:1891 (1953).

Stewart, C. W. Phys. Rev. 38:931 (1931).

Van Vleck. Phys. Rev. 74:1168 (1948).

Zezewski, M. Z. Physik 40:153 (1927).

Zwetkoff. Acta Physichimica (USSR) 16:132 (1942).

VIII. APPENDIX

Preparation of the Azoxy Compounds

Azoxy compounds can be prepared by various ways[1] :

I. Reduction of nitrophenol ether with glucose and sodium hydroxide

II. Per acetic acid oxidation of respective azo compounds

Reactions involved in the first method are:

(a) $_2ON\text{-}C_6H_4\text{-}OH \xrightarrow[\text{or Na in absolute alchol}]{NaOH} Na\,O\text{-}C_6H_4\text{-}NO_2$

(b) $_2ON\text{-}C_6H_4\text{-}ONa \xrightarrow{RX} RO\text{-}C_6H_4\text{-}NO_2 + NaX$

(c) $RO\text{-}C_6H_4\text{-}NO_2 \xrightarrow[80^\circ C]{25\%\ NaOH + Glucose} RO\text{-}C_6H_4\text{-}N{=}N(O)\text{-}C_6H_4\text{-}OR$

where Rx is the alkyl halide group.

I. (A). Etherification of p-nitrophenol.

24 gm of Na metal was dissolved in 500 cc of absolute alcohol. One mole of p-nitrophenol was put in a three-necked flask and 50 cc of absolute alcohol was added. The Na metal solution was added while stirring. 1.5 moles of alkyl halides were added dropwise from a dropping funnel with thorough stirring. Then the mixture was allowed to reflux for 8 to 10 hours. The mixture was allowed to cool

1. Chemical Reviews 9:110 (1931).

and filtered. Excess alcohol was distilled off and the residue was extracted with ether and washed with 5 to 7 percent alkaline solution. Then the ether was distilled off and crystallized from alcohol.

(B). Reduction of p-nitrophenol alkyl ether[2,3]

One mole p-nitrophenyl alkyl ether was taken in a three-necked flask and 25 percent solution of 1.5 moles of NaOH was added while stirring. The temperature was raised to 80° C. and 1.5 moles of glucose was added slowly while maintaining temperature at 80° C. in 30 to 45 minutes. The mixture was filtered and washed with water. Then the precipitates were steam distilled to remove impurities; for example, an unreacted nitrophenyl alkyl ether or any side products. Then the product was purified further by recrystallization from alcohol and benzene. This method gives almost quantitative yield if temperature is maintained at 80° C and glucose is added with thorough stirring. Insufficient stirring or incorrect temperature reduces the yield considerably. 25% NaOH solution seems to be optimum.

II. The following reactions are involved in this method:

(a) 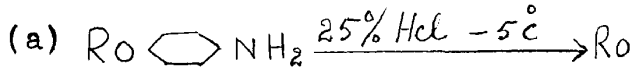

(b) 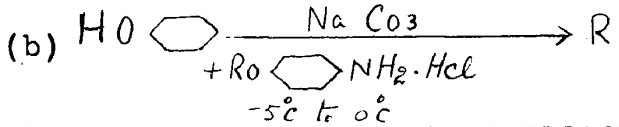

2. Can. J. Research 27B:890b (1949).
3. H. W. Galbraith, E. F. Degering and E. F. Hitch, J. Am. Chem. Soc. 73:1323 (1951).

(c) 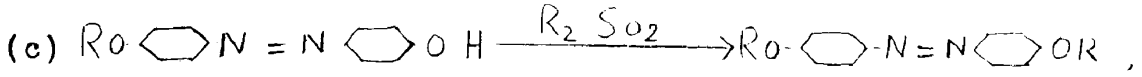

(d) 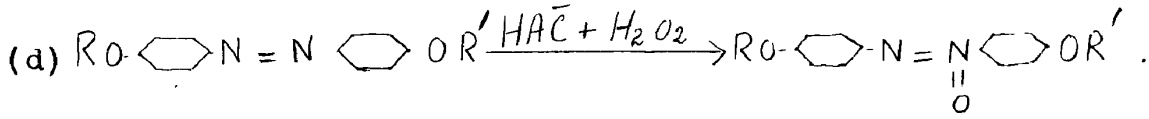

In the above method reaction steps (a), (b), and (c) give theoretical yields, but the reaction product in (d) is very susceptible to light in presence of excess HAc and H_2O_2. In sunlight it undergoes further oxidation very easily. The reaction product is very difficult to separate but this method was tried to obtain unsymmetrical azoxy compounds in which CH_3, C_2H_5 or C_3H_7 group combination is possible. Chromic anhydride oxidation of azo compound RO 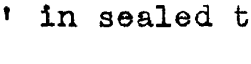 OR' in sealed tube is worthy of investigation.

---

4. Chemical Abstract 42:2588